Interpretation®

Morphology, internal architectures and formation mechanisms of mega-pockmarks on the northwestern South China Sea margin

Journal:	*Interpretation*
Manuscript ID	INT-2020-0175
Manuscript Type:	Technical Paper (if no special section applies)
Date Submitted by the Author:	13-Aug-2020
Complete List of Authors:	Lu, Yintao; Petrochina Hangzhou Research Institute of Geology Xu, Xiaoyong; Petrochina Hangzhou Research Institute of Geology Luan, Xiwu; Qingdao Institute of Marine Geology; Qingdao National Laboratory for Marine Science and Technology Jiang, Shu; China University of Geosciences Ran, Weimin; Qingdao Institute of Marine Geology; Qingdao National Laboratory for Marine Science and Technology Yang, Taotao; etroChina Hangzhou Research Institute of Geology Lu, Fuliang; PetroChina Hangzhou Research Institute of Geology Zhou, Yingfang; University of Aberdeen, School of Engineering Yang, Zhiliang; etroChina Hangzhou Research Institute of Geology
Keywords:	Asia, fluid, seafloor, seismic geomorphology, volcanics
Subject Areas:	Structural, stratigraphic, and sedimentologic interpretation

SCHOLARONE™
Manuscripts

Morphology, internal architectures and formation mechanisms of mega-pockmarks on the northwestern South China Sea margin

Yintao Lu[a]*, Xiaoyong Xu[a], Xiwu Luan[b,c], Shu Jiang[d], Weimin Ran[b,c], Taotao Yang[a], Fuliang Lyu[a], Yingfang Zhou[e], Zhili Yang[a]

a Petrochina Hangzhou Research Institute of Geology, Hangzhou, China, 310023;

b Qingdao Institute of Marine Geology, Qingdao, 266071, China

c Function Laboratory of Marine Mineral Resources, Qingdao National Laboratory for Marine Science and Technology, Qingdao, 266237, China

d China University of Geosciences, Wuhan, 430074, China

e University of Aberdeen, Aberdeen, AB24 3UE, United Kingdom

*corresponding author: Yintao Lu, Petrochina Hangzhou Research Institute of Geology, No.920, Xixi Road, Hangzhou, 310023, China. E-mail address: luyt_hz@petrochina.com.cn

For Peer Review

Abstract

Pockmarks, as depression morphology related to fluid escape on the seafloor, are revealed by three-dimension (3D) seismic data on the northwestern South China Sea (SCS) margin. The pockmarks can be classified into two groups by their various shapes in plan-view, which are circular group and elongating group. These pockmarks in the study area could be defined as mega-pockmarks, as their maximum diameters can reach to 7.5 km. They commonly develop more than one crater, which are central crater and secondary crater. The seismic data illuminated their complicated internal architectures in the subsurface, as well as their evolution periods, such as initiation stage, mature stage and abandonment stage. According to the buried structures and their genesis mechanism, the mega-pockmarks could be classified into linear faults-associated pockmarks and volcano-associated pockmarks. The linear faults-associated pockmarks root on the top Middle Miocene, where the linear faults distribute. The linear faults on the top of fluid reservoir in Middle Miocene act as conduits for fluid seepage. The fluid seepage is driven by the break of balance between the hydrostatic and pore pressure. When the fluid seepage initiate, they will migrate along the linear faults, making the linear feature of pockmarks on the seafloor. Both thermogenic gas from deep intervals and biogenic gas in shallow intervals may be fluid source for the genesis of pockmarks. On the other hand, the volcanic activities control the genesis and evolution of volcano-associated pockmarks. The volcano-associated pockmarks root on the craters of volcanoes. The volcanoes underneath the pockmarks provide volcanic hydrothermal solutions, such as phreatomagmatic eruptions through the volcanic craters. The confined fluid seepages make the pockmarks on exhibiting more circular shape on the seafloor. Long-term, multi-episode fluid expulsions generate the complicated internal architecture that leads to multi-cratered mega-pockmarks on the northwestern margin of SCS.

Keywords

Pockmarks; Linear faults; Volcano; Fluid seepage; South China Sea

For Peer Review

Introduction

Pockmarks, as depression morphology related to fluid escape on the seafloor, are widely identified on the present seafloor at a wide range of water depths all around the world (Bertoni, et al., 2019; Tasianas, et al., 2018; Maestrelli, et al., 2017; Krämer, et al., 2017; Cartwright and Santamarina, 2015; Sun et al., 2011a; Moss and Cartwright, 2010; Judd and Hovland., 2009; Cartwright, et al., 2007). Pockmarks with various shapes are commonly observed to be circular- to elongate-shaped, conical crater-like depressions, with numerous irregular shapes being described as well (Cole et al., 2000; Hovland et al., 2002). The dimensions of pockmarks could reach to very large scale, which are defined to mega-pockmarks. The diameters of mega-pockmarks are generally greater than 1000 m, and with depth more than 150 m (Pilcher and Argent, 2007).

Because the fluids from the subsurface supplied by various geological structures and different migration conduits, pockmarks are of great significance in studies of marine biology (Harris et al., 2012; Decker et al., 2010; King and MacLean, 1970), diapirs (Hovland and Judd, 1988; Hovland, 1991, 1992; Dimitrov and Woodside, 2003; Pilcher and Argent, 2007; Rowan et al., 1999; Whelan et al., 2005), deepwater sedimentology (Wenau et al., 2017; Judd and Hovland, 2009; Pilcher and Argent, 2007), climatology (Mazzini et al., 2017; Wenau et al., 2017; Riboulot et al., 2014), ocean bottom currents (Picard et al., 2018; Sun et al, 2011a; Anderson et al., 2008), geohazards (Hovland et al., 2002; Tjelta et al., 2007), deepwater gas hydrates (Lu et

For Peer Review

al., 2017; Riboulot et al., 2016), and oil and gas exploration (Nicholas et al., 2015).

The newly formed pockmarks are normally considered to have a flat-bottomed cone shape, due to slumping or the deposition of fine-grained sediment, that may develop over long time periods (Gay et al., 2006a, b; Pilcher and Argent, 2007). In contrast, paleo-pockmarks are those in which formation activity has ceased, i.e. fluid expulsion is not active, buried by younger sediments (Hovland, 1982; Cole et al., 2000; Games, 2001; Gay et al., 2003, 2006a, b; Pilcher and Argent, 2007). According to spatial arrangement, distribution, related underlying geology or local disturbance of the seafloor, and genesis mechanisms, the pockmarks could be defined into several classes, and the controlling factors for their genesis could be attributed to fault-strikes, buried channels, mud diapirs, slump, currents and icebergs (Pilcher and Argent, 2007).

Pockmarks on the northwestern margin of South China Sea (SCS), adjacent to study area, have previously been identified using high resolution seismic data and bathymetric data (Sun et al., 2011a; Chen et al., 2015). This discovery also reveals the great scale of pockmarks, of which diameter could reach to 3.31 km. Meanwhile, the potential formation mechanisms of the mega-pockmarks on the northwestern margin of SCS have been proposed to be reaction between the fluid seepages and bottom currents (Sun et al., 2011a; Chen et al., 2015). However, due to the limited coverage of multi-beam bathymetric and seismic data, there are still numerous mega-pockmarks have not been identified in this area. Furthermore, the buried

For Peer Review

structures in subsurface which control the genesis of pockmarks, and relationship between pockmarks and the buried structures, have not been have not been identified and analysed yet (Lu et al., 2017).

In this study, we describe and analyze, for the first time, 27 mega-pockmarks on the NW SCS margin using high-resolution 3D seismic data. These mega-pockmarks display various shapes on the seafloor and they have diameters of up to 7.5 km, which are much larger than those documented by the previous studies in the South China Sea (Sun et al., 2011; Chen et al., 2015) and other continental margins worldwide (Hovland and Judd, 1988; Fader, 1991; Foland et al., 1999; Haskell et al., 1999; Pilcher and Argent, 2007). The morphology, internal architecture and formation mechanisms of these mega-pockmarks have been revealed in detailed in this study. Meanwhile, according to the facies and geological structures identified under the pockmarks, two different categories pockmarks have been classified, and the different stages of their evolution have been reconstructed. The buried structures and associated pockmarks imply that linear faults in top of Middle Miocene and volcanic activities controlled the genesis and evolution of the pockmarks. The multi-episode evolution of the pockmarks represents fluid expulsion events in the NW SCS, which create the world-class scales and complicated internal architectures of mega-pockmarks.

For Peer Review

Geological setting

The study area is located in the northeastern part of Zhongjiannan Basin (ZJNB), adjacent to Qiongdongnan Basin (QDNB), between the Guangle Platform (GLP) and the Xisha Platform (XSP), where the water depth varies from 1,000 m to 1,500 m (Figure 1). The geologic framework of the study area is complex, having experienced strong tectonic movements since the Early Tertiary, primarily due to northeast-directed extensional activity (Lüdmann et al., 2005; Yan et al., 2006). Tectonic activity along the western margin of the basin formed the NW-striking Red River Fault Zone (RRFZ), which is the boundary fault zone of the SCS. The XSP and GLP formed in the Neogene, during which time the Xisha Uplift and Guangle Uplift developed (Fyhn et al., 2009; Ma et al., 2011; Sun et al., 2011a). Both the XSP and GLP are active and developing carbonate platforms, comprised of large atoll- and patch-reefs (Ma et al., 2011). The complex topography of the seafloor in the study area has experienced substantial recent alteration by bottom currents (Sun et al., 2011a).

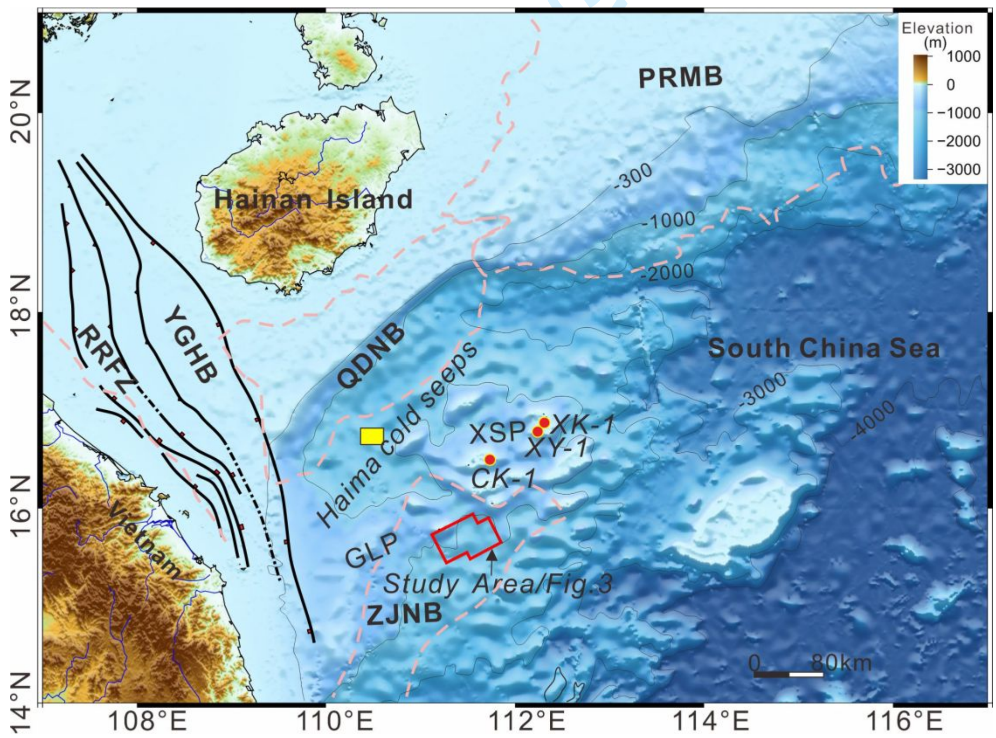

Figure 1 The study area (red rectangle), located to the south of Qiongdongnan Basin and the west of Zhongsha Uplift, with a water depth ranging from 1000 to 1,500 m. ZJNB: Zhongjiannan Basin; QDNB: Qiongdongnan Basin; PRMB: Pearl River Mouth Basin; YGHB: Yinggehai Basin; RRFZ: Red River Fault Zone. The yellow boxes indicate the locations where fluid samples were collected.

The depositional history of the study region has been divided into two mega-sequences based on tectonic activity: a period of rifting in the Eocene–Oligocene, and a post-rift period in the Miocene–Quaternary (Figure 2; Xie et al., 2006). The Paleogene stratigraphy of the rift stage mega-sequence is composed of three formations, which have a total thickness of several kilometres (Xie et al., 2006; Zhu et al., 2009). These sediments, specifically the Lingtou Formation deposited in the Eocene, and the Yacheng and Lingshui Formations deposited in the Oligocene, are characterized by lacustrine facies mudstones, neritic mudstones and coastal plain coal-bearing strata, which serve as source rock for thermogenic gas in petroleum systems (Figure 2; Huang et al., 2003; Xie et al., 2006; Zhu et al., 2009).

For Peer Review

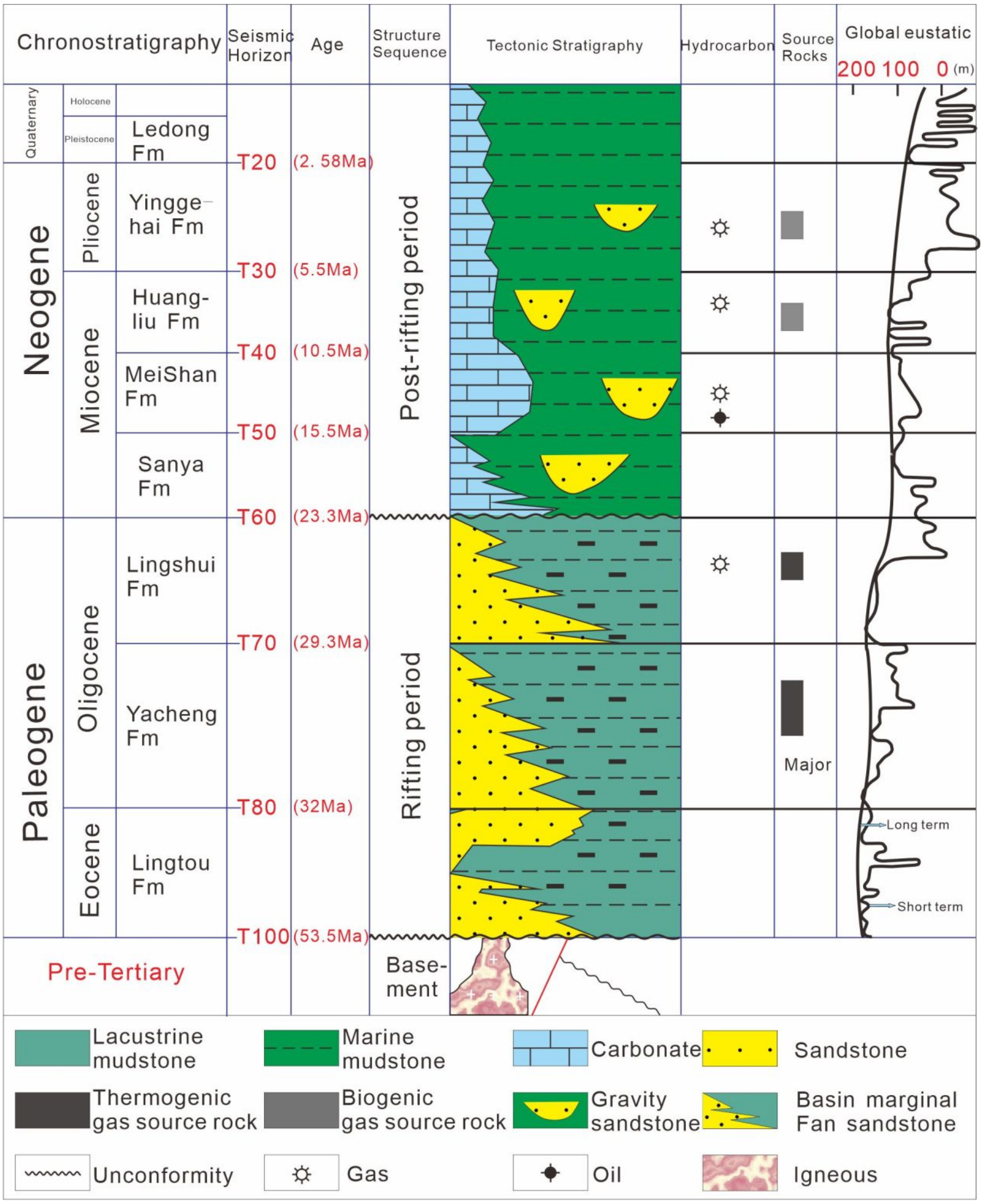

134

135 **Figure 2 Generalized chronostratigraphic chart of the study area and adjacent**
136 **area (after Xie et al., 2006; Zhu et al., 2009; Sun et al., 2010) showing the**
137 **sequence stratigraphic horizons used in study. The global eustatic sea level data**
138 **and sea level change data used in this study were adopted from Haq et al. (1987)**
139 **and Miller et al. (2005), respectively. Fm: Formation.**

The Neogene stratigraphy can be further divided into four formations, which are dominated by hemipelagic-pelagic deposition (e.g., Xie et al., 2006; Sun et al., 2010, 2011a). These sediment intervals provide significant hydrocarbon reservoirs for the petroleum system in northern SCS (Xie et al., 2006; Sun et al., 2010, 2011a; Lu et al., 2017). Among the reservoirs, the carbonate reservoir in Middle Miocene represents a carbonate development event in northern SCS, especially distributed in the carbonate platforms successively developed on the paleo-uplifts (Xie et al., 2006; Lu et al., 2017).

The relative change in seafloor in the SCS coincides with the global relative seafloor change after 5.7 Ma (Figure 2; Zhao et al., 2001). The target interval used in this study was deposited during the post-rift thermal subsidence stage, when tectonic activity was relatively weak (Zhou et al., 1995). However, neo-tectonic movement has continued since the late Miocene, and is associated with the collision between Taiwan and the mainland Chinese continent, as well as the change in movement direction of the RRFZ (Lüdmann and Wong, 1999). One consequence of the recent tectonic activity has been the generation of igneous intrusions. The emplacement of the intrusions has produced high heat flow in the area, which started in the late Miocene (Yan et al., 2006; Sun et al., 2011a), and has driven regional uplift and erosion (Fyhn et al., 2009).

Besides these events, polygon faults in the Meishan and Huangliu Formations have also played an important role in the evolution of sedimentary sequence in

For Peer Review

Neogene (Sun et al., 2009, 2010). The sediment was dominated by fine-grained muddy and silty pelagic and hemipelagic deposits after the Middle Miocene (Lu et al., 2011, 2017; Sun et al., 2012), providing comfortable condition for the genesis of polygonal fault system (PFS) (Cartwright et al., 2003; 1999). The processes for formation of polygonal faults, such as dewatering and compaction processes (Cartwright et al., 1999; 2003) would result in porosity changes in bulk sediment as well as fluid supply for sediment environment.

Materials and Methods

High quality 3D seismic data in the study area were acquired in 2011. Seismic data was processed with bin spacings of 12.5 m and 25 m in line and crossline directions, respectively. The sampling interval was 2 ms, and the dominant frequency (< 2 s two-way time, TWT) was 50 Hz, with the vertical resolution of about 10 m.

High resolution topography of the seafloor (Figure 3), including pockmarks was extracted by seismic interpretation in 1-line by 1-trace grid. Other seismic horizons, such as T40, T30, and T20, were also acquired by seismic interpretation. The detailed geometry of pockmarks is displayed by 3D visualization technology, demonstrating the internal architecture, as well as the contact relationship with surrounding strata.

Seismic dip and coherence attributes were extracted by using interpolated seismic surfaces. Figure 3a shows the geometry of the seafloor as calculated from seismic horizons using a water velocity of 1500 m/s. Figure 3b shows the dip extracted from the seafloor horizon. The coherence attribute was used to identify the

For Peer Review

plane distribution of faults, subtle sedimentary features, as well as pockmarks in subsurface. Polygonal faults were also identified in seismic sections and displayed by using coherence attribute in map view.

Morphology study has been used in this study, to differentiate various shapes of different pockmarks. The higher shape factor value means more circular shape, while the lower value means more linear shape.

For Peer Review

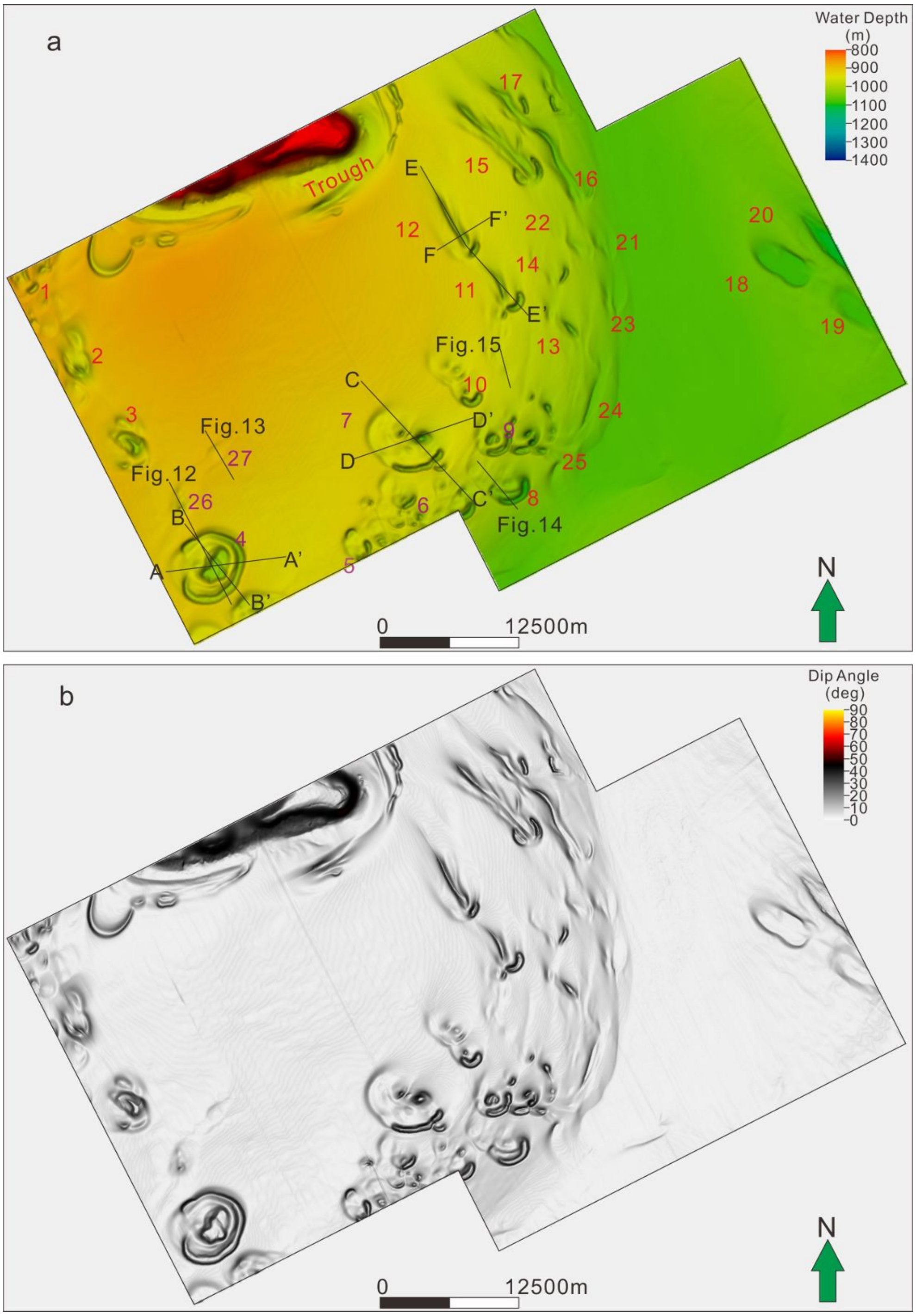

Figure 3 a) Shaded relief map of seafloor calculated from 3D seismic data using a water velocity of 1500 m/s, showing the distribution of pockmarks in this area. The red labels numbers represent the pockmarks associated with buried volcanoes; the purple labels numbers represent the pockmarks associated with linear faults; b) seafloor dip map extracted from seismic data.

Results

Morphology of mega-pockmarks

The 3D seismic data reveals densely distributed depression features in the study area. These depressions are pockmarks, according to their similar plan-view shapes and section profiles with other pockmarks all around the world (Bertoni, et al., 2019; Tasianas, et al., 2018; Maestrelli, et al., 2017; Krämer, et al., 2017; Lu et al., 2017; Cartwright and Santamarina, 2015; Sun et al., 2011). These depressions commonly develop giant size, with diameters > 6,000 m, or lengths > 8,000 m on the seafloor, with various shapes. The scale of these giant depressions is several times larger than those pockmarks reported previously (Hovland and Judd, 1988; Fader, 1991; Foland et al., 1999; Haskell et al., 1999; Pilcher and Argent, 2007), including those classified as giant pockmarks in the adjacent area (Sun et al., 2011). Therefore, these depressions are defined as mega-pockmarks (Figure 4).

The acreage of individual mega-pockmarks in study area ranges from 1 km^2 to 31.7 km^2 (Figure 5), with the length of long axis ranges from 1.5 km to 12.8 km (Figure 4). The largest pockmark, D4, locates in the southwest of the study area, reaches 31.7 km^2 in area and 223 m in depth (Figure 5, 6). D16, locates in the northeast of the study area, has developed the greatest long axis length, which reaches 12.8 km. The water depth of the base of pockmarks on the seafloor ranges from 996 m to 1,358 m, with an average water depth of 1,225 m. The depth of mega-pockmarks varies across a wide range from 21 to 223 m (Figure 6).

For Peer Review

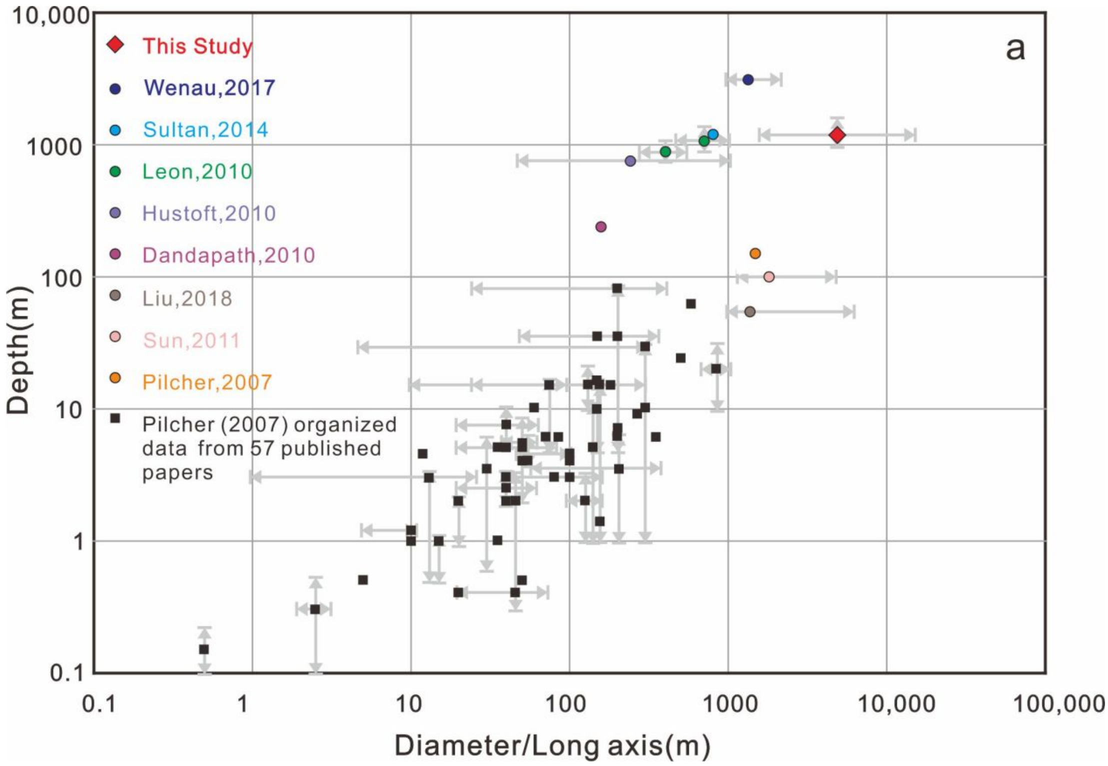

Figure 4 Dimensions of mega-pockmarks on the seafloor in the study area. Log-log plot showing the relationship between diameter or long axis and depth of pockmarks, throughout the world and in the study area. The pockmarks in the study area are larger than any others discovered globally.

The variety of the morphology of pockmarks on seafloor indicates the unique structural and sedimentary feature. The pockmarks could be divided into circular and linear ones by their plan-view, and they have different shape factor values (Figure 5). Some of the depressions exhibit circular and semi-circular shape, very similar to the shape of pockmarks observed globally on the current seafloor (Hovland, 1982; Cole et al., 2000; Games, 2001; Gay et al., 2003, 2006a, b; Pilcher and Argent, 2007; Sun et al., 2011a; Lu et al., 2017). Another group of pockmarks exhibit more linear features, which show some crescent-like (such as D13, 14), elliptical (such as D2, 10, 18, 19), and irregular shaped (such as D11, 17) depressions.

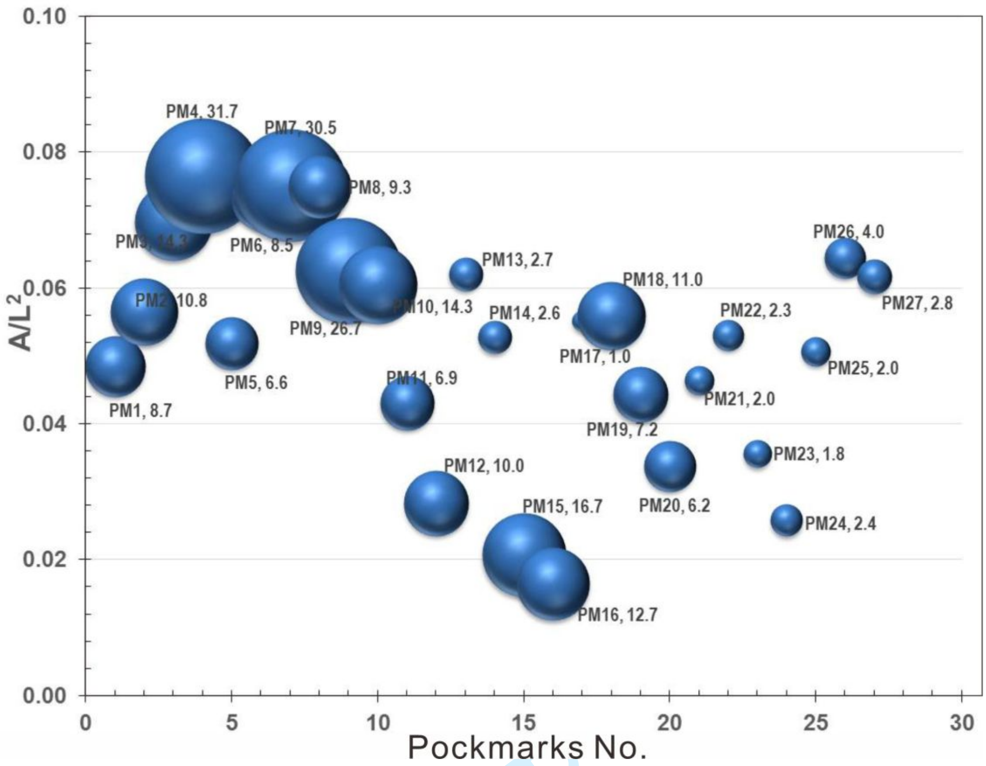

Figure 5 Plot of shape factor (area/perimeter^2) against number of pockmarks in the study area. The bigger pockmarks are represented by larger spheres. The number of pockmarks is followed by their acreage.

Review

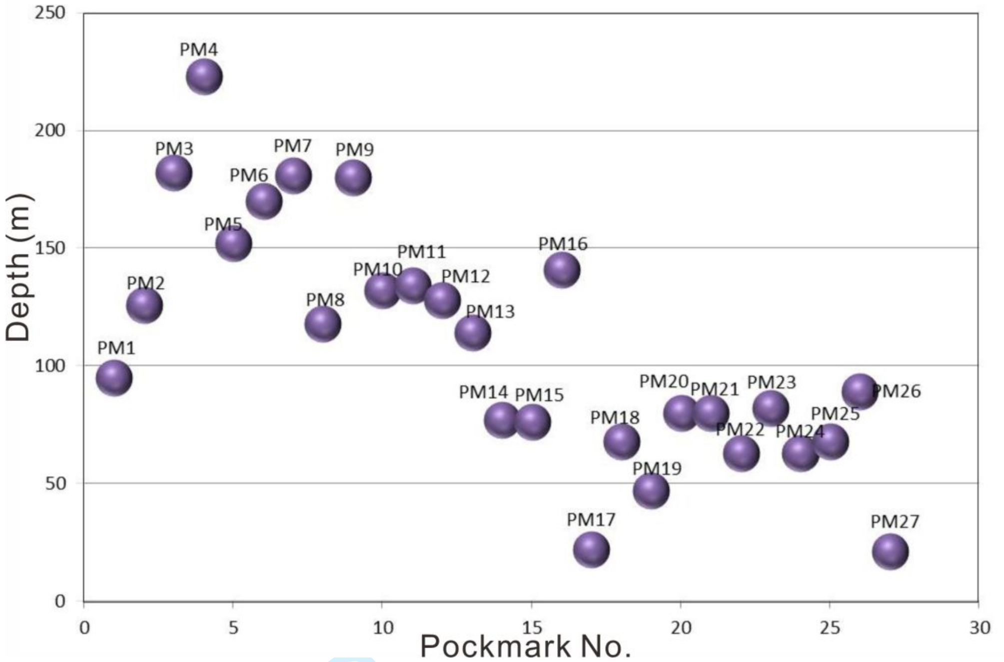

Figure 6 Plot of depth of the pockmarks' bases against number of pockmarks in the study area. The depth of pockmarks range mainly from 50 m to 200 m.

For Peer Review

The depressions have commonly developed more than one crater, with secondary craters forming around the margin of a single central crater (Figure 7). These characteristics are most obvious among the circular depressions, especially D3, D4, D7, D8, and D9. Elongated depressions also exhibit central craters, but these have developed as a relatively crescent-shaped trough at the front of the main structure, e.g., D11, D12 and D15. Secondary craters express asymmetrical features, with a deeper base on the down slope side, and a shallower base on the up-slope side.

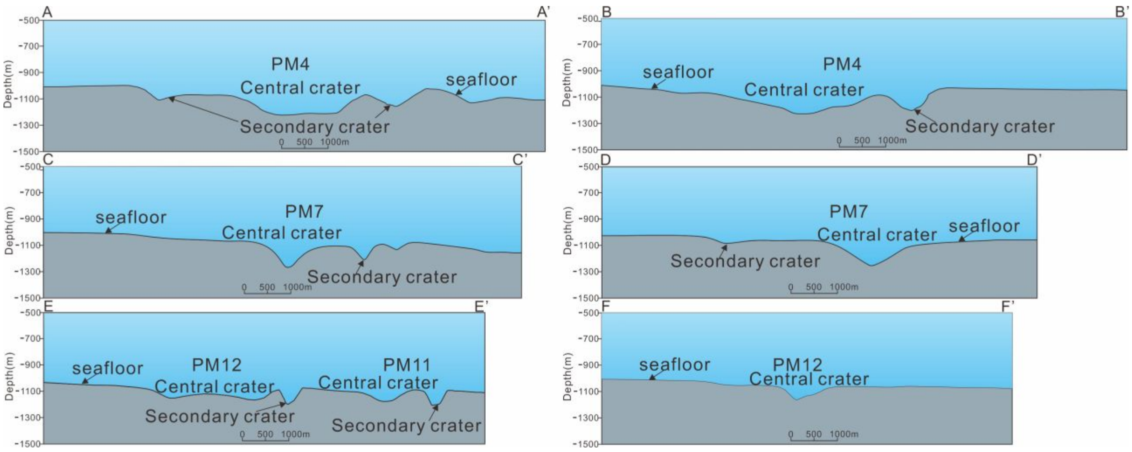

Figure 7 Diverse profile features of pockmarks on the seafloor. Depressions in the pockmarks exhibit a range of shapes. The pockmarks normally develop secondary craters alongside central craters. The secondary craters generally develop asymmetrically around the margins of pockmarks, with a steeper wall on the basinward side. See the location in Figure 3.

The pockmark morphology is mainly distributed around margin of platform, while it is absent on the central platform (Figure 3). Furthermore, the circular pockmarks tend to have developed in the west of the study area, while linear pockmarks are more common in the east of the study area. Moreover, the long axes of elliptical pockmarks are generally oriented northwest to southeast (Figure 3).

Internal architectures of mega-pockmarks

High-resolution 3D seismic data revealed subsurface depression features. The roots of depressions can be identified in the subsurface at 1,900 ms, about 550 m below the seafloor, assuming the seismic velocity of the shallow intervals to be 2,200 m/s. As shown in Figure 8 and Figure 9, the internal architectures of both circular and linear-shaped group of pockmarks are very complicated and thus their shape couldn't

For Peer Review

be characterized by simple “U” or “V” shaped profiles. The boundaries between pockmarks and surrounding strata are very sharp as identified by differential seismic reflection. The reflectors inside pockmarks could be correlated with surrounding strata, although the sediment thickness within the depressions is marginally greater than the same layers in the surrounding strata. Meanwhile, the architectures between them are quite different. The surrounding strata is characterized by horizontal, parallel and higher frequency reflection, while the internal strata are featured by undulate and lower amplitude reflection, locally developing chaotic reflectors. The deformation is common inside pockmarks, with dim reflection, indicating slumping and sliding during depression formation. Furthermore, the sliding feature, and differential reflections between pockmarks and surrounding strata imply the boundaries are sliding planes.

For Peer Review

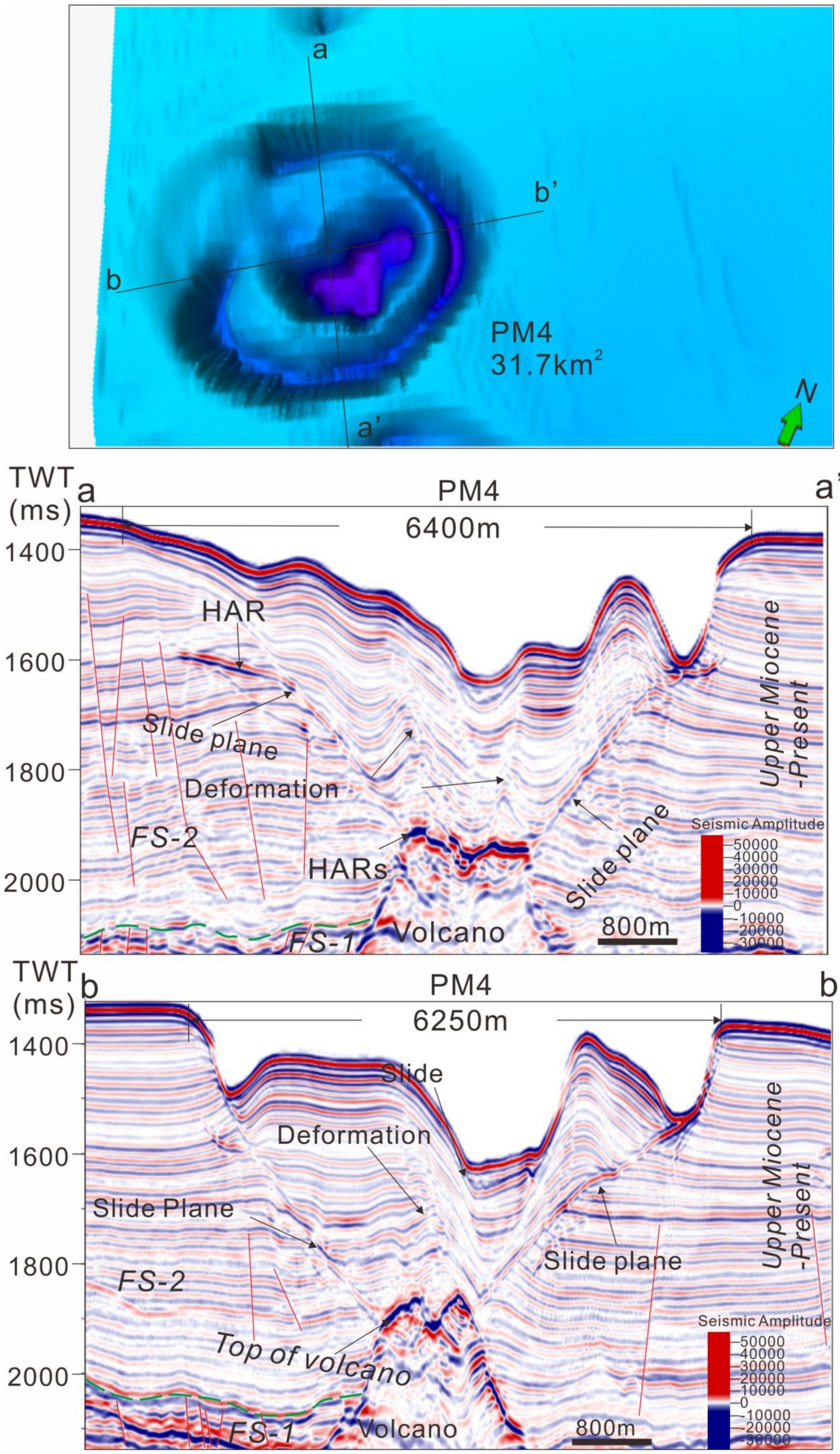

Figure 8 3D visualization view and seismic sections across typical circular pockmark PM4. The seismic sections reveal the complicated topography on the

276 **seafloor and the inner architecture of PM4. Pockmark size is marked on the**
277 **maps and seismic sections. FS: fault system; HAR: high amplitude reflectors. See**
278 **Figure 3 for the locations of PM4.**

279 Some high amplitude reflectors (HARs) could be recognized close to pockmarks,
280 which could be tracked to sliding planes (Figure 8, 9). Meanwhile, some pipe-like
281 reflectors could be identified inside pockmarks, from root onto seafloor. They exhibit
282 transparent feature, even with pull-down characteristic (Figure 9).

For Peer Review

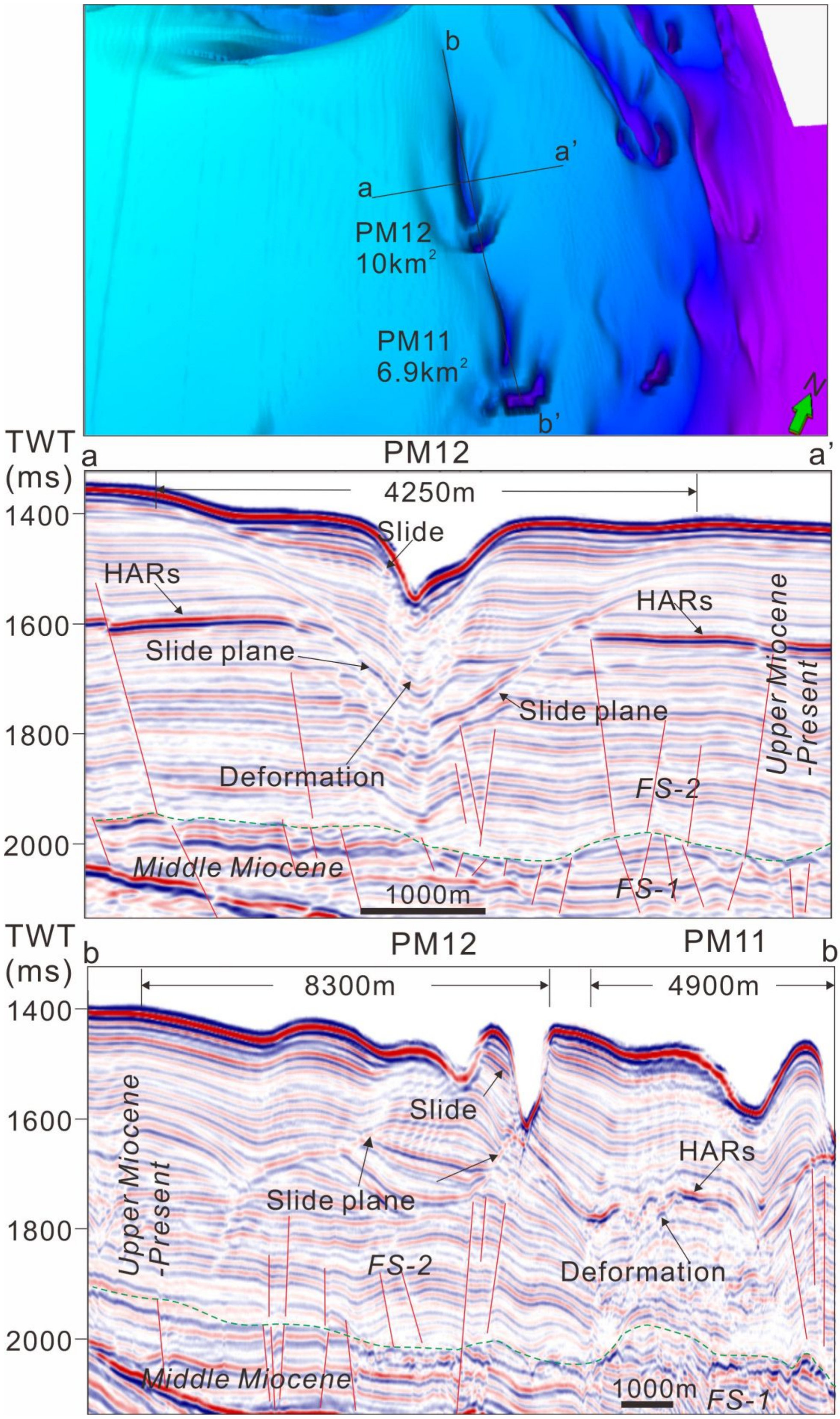

Figure 9 3D visualization view and seismic sections across typical linear pockmark PM12. The seismic sections reveal the complicated topography on the

seafloor and the inner architecture of PM12. Pockmark size is marked on the maps and seismic sections. FS: fault system; HAR: high amplitude reflectors. See Figure 3 for the locations of PM4.

Distribution of faults and buried volcanoes

Numerous, closely-spaced normal faults with small offsets were identified from the 3D seismic data. Two-tier fault systems could be identified in the seismic cross sections, developing in Middle Miocene and Upper Miocene to Pliocene, which are called FS-1 and FS-2 respectively (Figure 8, 9). These faults have developed associated small fault throw, and generally extend a limited distance, to form complicated fault network (Figure 10). The elder one, FS-1, terminates at seismic horizon T40, correlating to top Middle Miocene, which is dominated by carbonate deposition intervals as petroleum reservoirs (Sun et al., 2009, 2010; Lu et al., 2011; 2017). The younger one, FS-2, develops between seismic horizon T40 and T20, which correlates to Upper Miocene to Pliocene (Figure 2, 8, 9). Some pockmarks are rooted on the top of Middle Miocene, which can be identified in the seismic data (Figure 8, 9) and coherence slice (Figs.10). These faults divide the strata into numerous faulted blocks, which are characterized as high amplitude, low frequency, discontinuous reflectors in the seismic sections (Figure 8, 9).

The coherence attribute along top of Middle Miocene is extracted to obtain a plan-view of the fault systems (Figure 10a). The coherence attribute slices show that the linear faults are mainly distributed around the margin of platform, exhibiting

For Peer Review

higher density in the eastern and western parts of study area (Figure 10a). Faults strike dominantly NW–SE, with subordinate NE–SW-striking faults also present. The long axis of pockmarks on the seafloor also tend to be oriented mainly NW–SE (Figure 10a). Some of these faults, with typical polygonal planform geometry, are referred to polygonal faults (Figure 10c). The typical polygonal faults, as a part of FS-1, are developed at the top of Middle Miocene (Figure 8, 9).

The coherence slice at the top of Middle Miocene shows more direct and consistent relationships between linear faults with the pockmarks. Where the pockmarks are developed on the seafloor, seismic data shows related linear faults have developed underneath the pockmarks. In the central platform and the toe of slope, the density of faults is reduced, although the faults are still as arranged in typical polygonal planform geometry (Figure 10c). Besides the density of faults, the pockmarks are also absent where the polygonal faults developed.

Other pockmarks are rooted on just above the volcanoes, which are characterized by their hump or moundy shape, as well as sharp and high amplitude reflections boundaries between surrounding strata (Figure 8, 9). The inner architecture of volcanoes is characterized by chaotic, low frequent and with medium amplitude reflectors. The volcanoes strongly re-construct the surrounding strata, making the strata deformed. The volcanoes are widely recognized by seismic data in south part of the study area. They are characterized by low coherence value anomalies with circular

For Peer Review

or stripped shape in plan-view (Figure 10a, b). The diameter of top volcanoes could reach to more than 1 km, and their root could be tracked to very deep intervals.

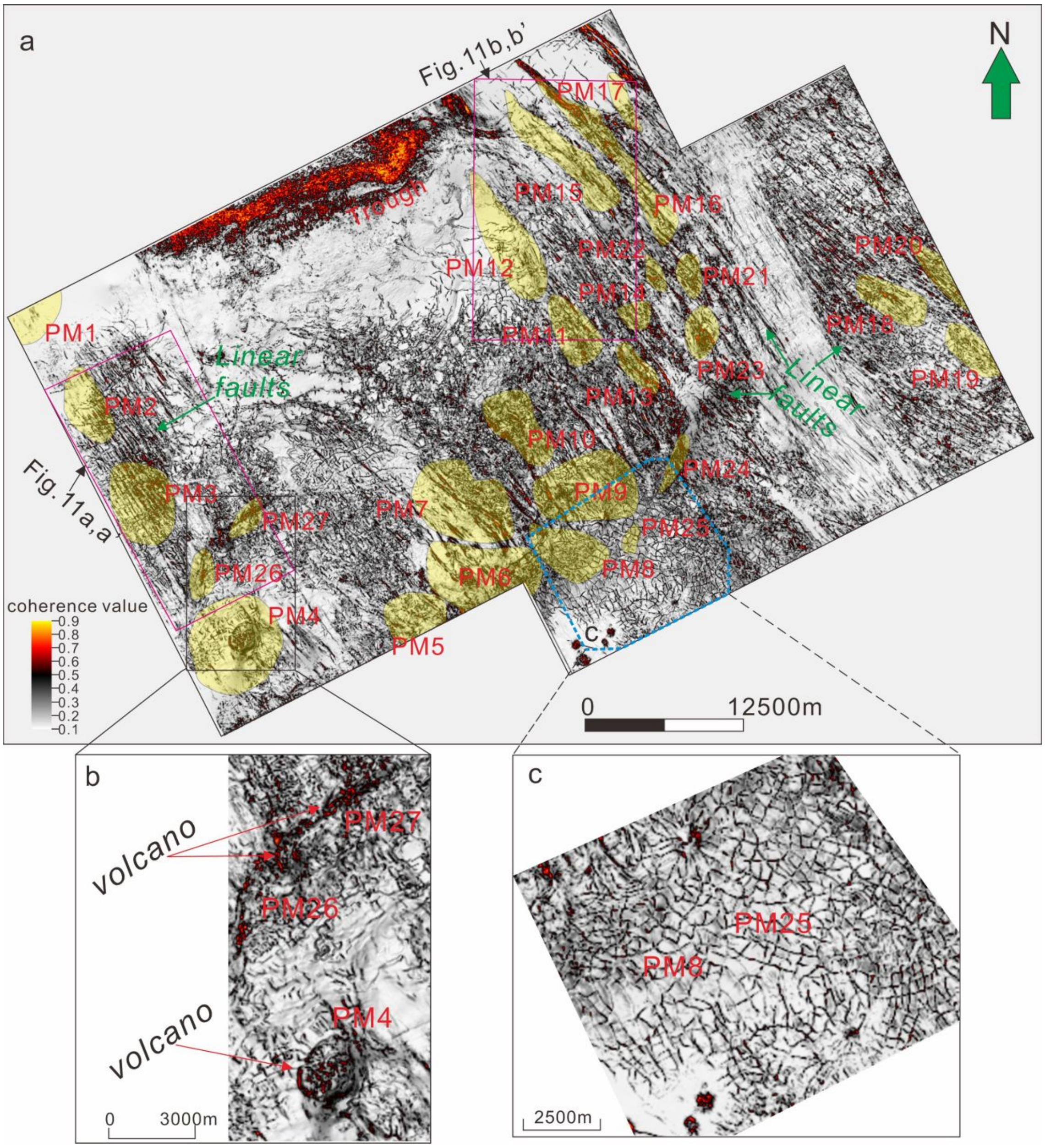

Figure 10 Seismic coherence slice of top Middle Miocene (T40), which shows the distribution of fault system and volcanoes. a) Pockmarks superimposed on coherence slices at the top of Middle Miocene, as the plan-view of FS-1. Oriented linear faults have developed around margin of platform, especially in the western and eastern regions, while typical polygonal faults have developed in the

central region and along the south edge. Pockmarks are developed where linear faults have a high density, especially where NW-SE striking linear faults are most abundant; b) Zoom-in coherence slice of typical volcanoes in southwestern margin of study area, which show round or stripped-shape of low coherence value; c) Zoom-in image of typical polygonal faults in toe of slope, which show less coincidence between polygonal faults with pockmarks.

Discussion

Pockmark classification

Although pockmarks express similar features on the seafloor, different types of pockmark have experienced a different evolution. According to the relationship between pockmarks and volcanoes or linear faults, the pockmarks have been classified to two major types; i) linear fault–associated pockmarks, and ii) volcano–associated pockmarks. In general, the linear fault-associated pockmarks have a lower shape factor value, in particular PM15 and PM16. The volcano-associated pockmarks have a higher shape factor value, e.g., PM4, PM6, PM7, PM26, and PM27 (Figure 3, 5).

Linear fault-associated pockmarks

Most depressions on the seafloor are rooted on the top of Middle Miocene, and show close relationship with linear faults, e.g., D1, D2, D3, D8, and D10–D25, which are classified as pockmarks associated with linear faults. They tend to exhibit

For Peer Review

elongated feature, such as crescent-like, elliptical, and irregular shapes in plan-view, with the long axis in NW-SE direction (Figure 3). They are mainly distributed around the margin of platform, especially in the eastern and northwestern parts of study area (Figure 10a). The occurrence and elongated axis of pockmarks has a high coincidence with dense linear fault distribution, along NW-SE direction (Figure 10). This NW–SE-oriented character was more emphasized along the western and eastern part of study area, and along the edge of the platform in the middle of study area, where the density of pockmarks is larger. Meanwhile, pockmarks are absent in the central platform and the basin floor, even in the area where the typical polygonal faults develop (Figure 3, 10). These linear faults acted as essential conduits for fluid escape (Pilcher and Argent, 2007), rather than polygonal faults. Therefore, the set of NW–SE faults in Middle Miocene can be classified as the conduits group.

For Peer Review

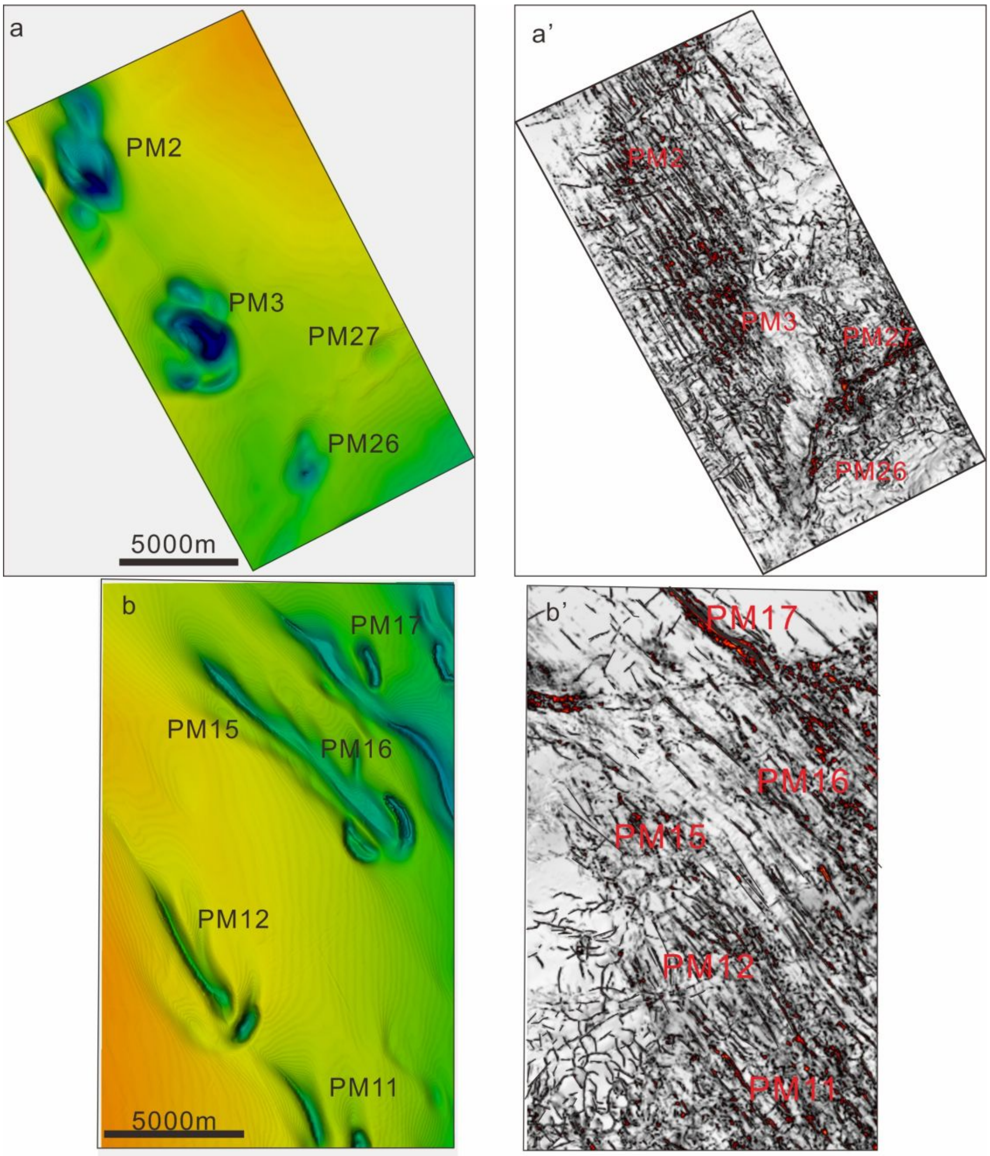

368

369 **Figure 11 Maps of pockmarks on the seafloor and the related coherence slices of**
370 **top Middle Miocene. The linear faults have consistently strike of NW–SE. The**
371 **distribution and direction of pockmarks have great coincidence with the linear**
372 **fault, except PM 26 and 27. The long axes of elliptical pockmarks are similarly**
373 **oriented in a NW-SE direction. See Figure 7 for map locations.**

374 ***Volcano-associated pockmarks***

375 Besides linear faults-associated pockmarks, other pockmarks are rooted at the
376 top of volcanoes (Figure 3, 8, 10), e.g., PM4, PM5, PM6, PM7, PM9, PM26, and

PM27, which are classified as volcano-associated pockmarks. Volcanoes were revealed to lie beneath these pockmarks in the seismic sections (Figure 8, 12). The pockmarks were densely developed in the southwestern part of the study area (Figure 3a, 10), having a larger scale and more circular shaped than pockmarks on the seafloor (Figure 3, 5).

The sediment sequences inside pockmarks are comparable with the surrounding strata (Figure 12, 13, 14), indicting the same sedimentary history. While on the other hand, the volcanoes should be active until very late time, even until recent (Lu et al., 2011; 2014). The volcanoes distribute along NE-SW direction, such as PM4, PM5, PM6, PM7, and PM9 in the south margin of 3D survey, and PM26 and PM27 in the middle-west part of study area (Figure 3, 10). For example, the volcanoes underneath PM26 and PM27 exhibit volcanic bend feature, distributed with NE-SW strike (Figure 10b, 11). The distribution pattern of volcanoes implies the volcanoes which are prolonged volcanoes in northern margin of SCS (Zhao et al., 2016, 2020), are aligned in NE-SW direction.

The volcano-associated pockmarks were very limited developed in the southern part of the study area (Figure 3a, 10). Most of the pockmarks above the volcanoes are randomly distributed, and have a larger scale and more circular shape than linear faults-associated ones on the seafloor (Figure 3). The scale of the volcano-associated pockmarks shows coincidence with the scale of the volcanoes underneath them, while the larger pockmarks relate to larger volcanoes (Figure 12). The seismic sections also

For Peer Review

reveal several volcano-associated pockmarks with smaller scales on the seafloor, as well as gentler deformation in subsurface, such as PM26 (Figure 3, 12) and PM27 (Figure 3, 13).

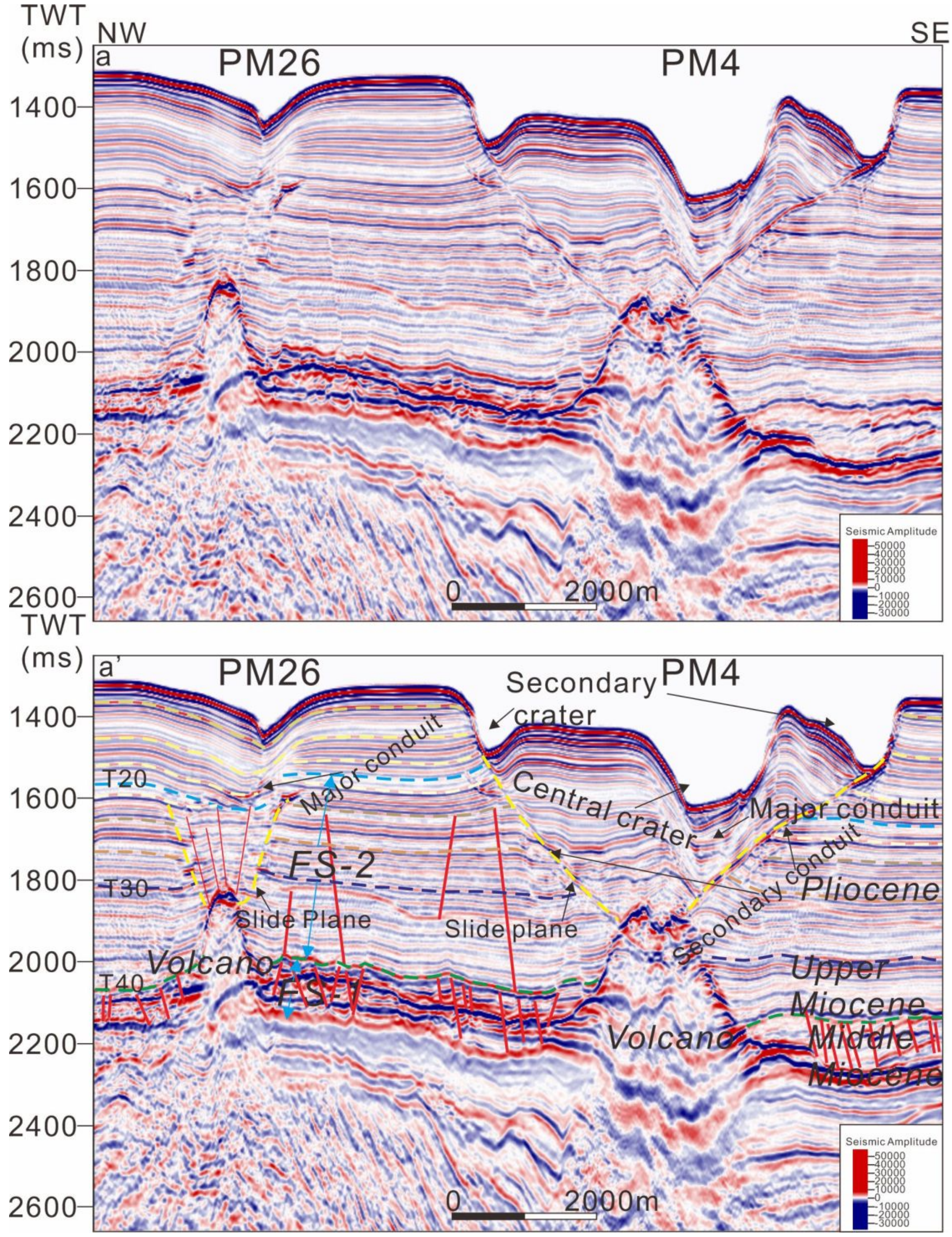

Figure 12 Seismic sections across diapir-associated pockmarks with interpretation, and associated plan views constructed from coherence slices. a) Plan view of the top of MFS-3.0; b) Plan view of the top of PFS-1; c) Seismic

section through PM4 and PM26; d) Interpreted seismic section through PM4and PM26. And the green horizon represents the top of PFS-1, while the blue horizon represents the top of PFS-2. See Figure 3 for map locations.

Initiation and evolution of mega-pockmarks

Analysis of the formation and evolution phases of pockmarks has been reported previously (Sun et al., 2011a; Chen et al., 2015; Lu et al., 2017; Wenau et al., 2017; Hovland, 1991; Hovland et al., 2002). However, direct observation of the stages of pockmarks evolution is still lacking. In the study area, different phases of pockmark development are revealed in the high resolution 3D seismic data, which have been termed the early, mature, and abandonment stages.

For Peer Review

Initiation stage

The initial stage of pockmark formation is expressed by gentle deformation of the seafloor, such as that associated with PM26 (Figure 12) and PM27 (Figure 13). The depth of crater of PM26 is about 75 m, while PM27 is 25 m, which is much smaller than others in the study area. Both PM26 and PM27 appear as low relief depressions on the seafloor, with elliptical outlines. A volcano can be identified beneath PM27 (Figure 13), indicated by a mound with a conical shape. Several fault-like features have developed above the top of the volcano, exhibiting funnel shape, which is Initiation stage of volcano-associated pockmark.

The seismic horizon T20 divides these funnel shape structure, as early stage pockmark, into two parts (Figure 13). Within the lower part, the fault-like features are denser than the upper group, while they are characterized by dip dim reflections. This funnel shape early stage pockmark is capped by HARs, where fault-like features terminate. These HARs are interpreted into shallow gas or fluid accumulation, while these dip fault-like features are fluid conduits for fluid migration (Figure 13). The upper part of this pockmark also develops HARs, indicating fluid accumulation as well. However, the upper part of this pockmark exhibits much clearer features, lacking chaotic reflectors, as well as lacking fluid conduits. The observation of two parts of PM27 implies that most of the fluid did not migrate to the seafloor, but mainly remained trapped in the lower section, while some portions seeps into the upper part. This also resulted in the gentle deformation in the upper part, and negligible deformation on the seafloor. Therefore, the processes could not create noticeable depression on the seafloor, differential with the seafloor where the pockmarks develop. PM27 is regarded as initiation stage pockmark, since its lack of fluid seepage and gentle deformation for the sediment intervals.

For Peer Review

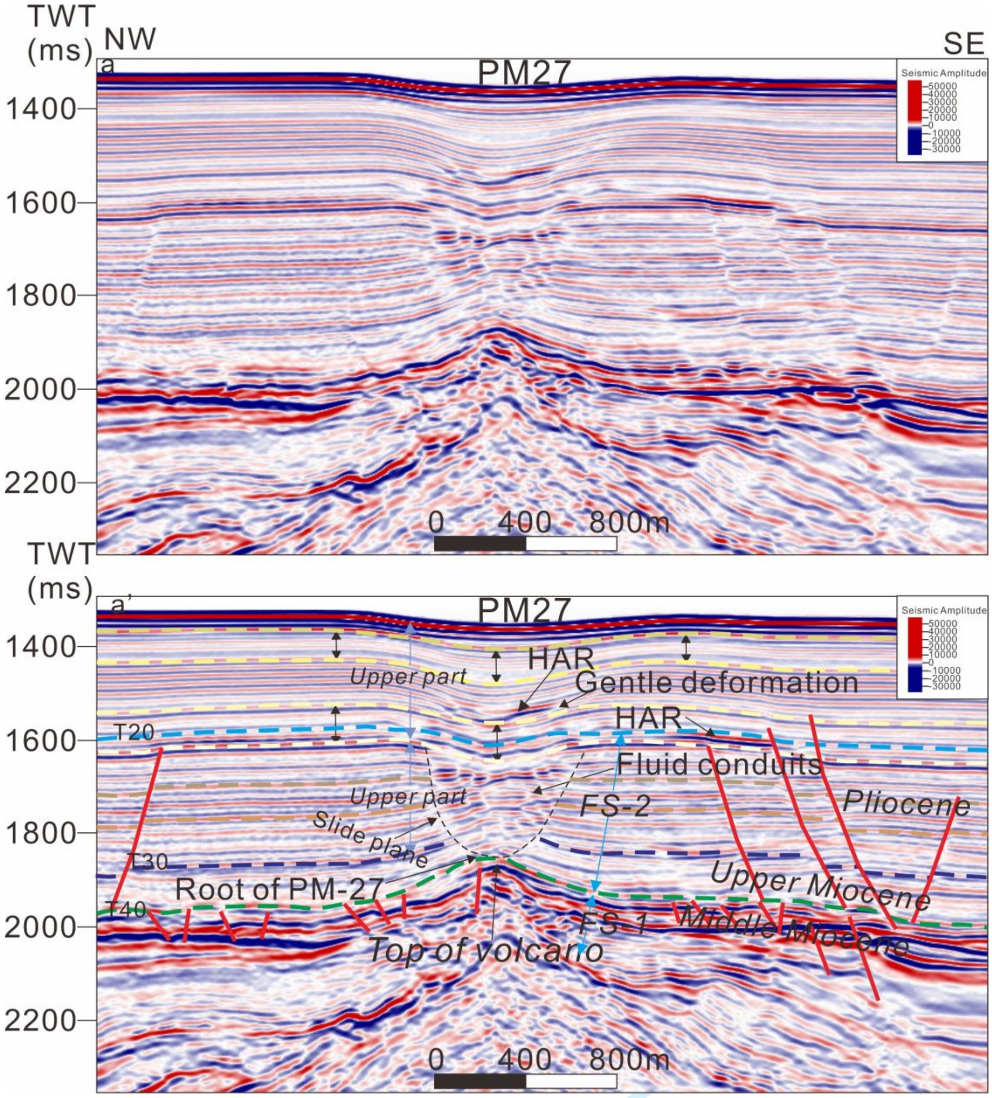

Figure 13 a) Seismic section across early phase pockmark 27; b) The same seismic section with interpretation. The green horizon represents the top of polygonal fault system 1 (PFS-1), while the blue horizon represents the top of polygonal fault system 2 (PFS-2). See Figure 3 for location.

Mature stage

Most pockmarks in the study area are currently in the mature phase, generally rooted on linear faults or on top of volcanoes, exhibiting strong deformation and slumping. As shown in Figure 14, the fault systems below these mature pockmarks are much more complex than pockmarks in the initiation stage. The deformation and sliding features are common inside pockmarks, which are characterized by chaotic reflectors, especially in the lower part or root of pockmarks.

As shown in Figure 12, the boundary of PM8, as sliding plane, is characterized by continuous and high amplitude reflection. Some HARs are recognized close to boundary of PM8, even on the seafloor, indicating gas or fluid accumulation. These fluid seepage and accumulation features indicate sliding plane act as major fluid conduits. A vertical pipe-like dim reflector could be identified inside PM8, from middle part onto seafloor. This pipe is also regarded as minor conduit for the fluid seepage, causing gentle depression on the seafloor. There are probably two conduits for fluid migration; one in the central area of the pockmark, while another at the boundary of the pockmark, especially in the basinward direction. Accordingly, more than one crater can develop in mature pockmarks, in both the central and marginal areas. Figure 14 shows the shallow subsurface interval of the central area has been strongly deformed, which is consistent with crater formation on the seafloor.

Some pockmarks, such as PM8, show migration features in seismic sections; these pockmarks are similar to pockmarks observed in the Western Mediterranean, and could be interpreted to form as the result of fluid activity (Riboulot et al., 2014). As presented in Figure 3 and 14, PM8 is located in a slope environment, with a ring-shaped crater in the downslope direction. PM8 generally dips towards the downslope direction, with its root oriented in the upslope direction. A basinward slide

For Peer Review

plane was identified in the seismic section, dipping to SE direction. The slide plane acts as the boundary of PM8, with seismic reflectors terminating in this plane. Several paleo-slide planes could be identified by their chaotic reflectors, which reflect slumping, sliding, or deformation processes. The architecture of PM8 is characterized by different funnel-like features, which are filled with parallel reflectors, and interbedded with chaotic and deformation reflectors. A vertical but minor conduit could be identified in the centre of PM8, associated with a low relief depression on the seafloor.

For Peer Review

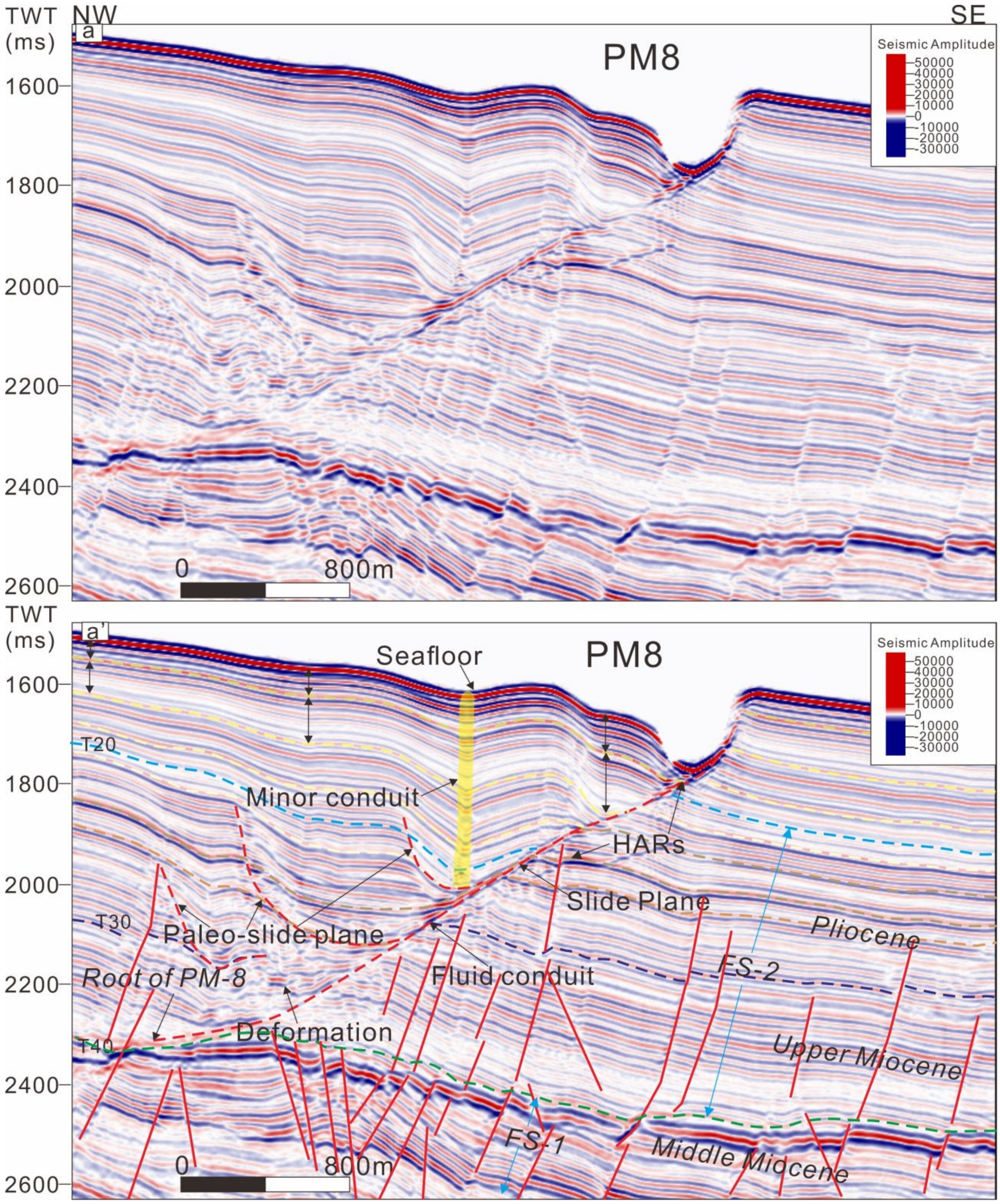

Figure 14 a) Seismic section across PM8, a mature phase pockmark which exhibits a complicated inner architecture. b) The same seismic section with interpretation. The different stages e.g. Stage-1 and Stage 2 were picked in seismic section, and tracked into horizons. The boundary of the pockmark was confined by the slide plane, which also acted as fluid migration path, or fluid

conduit. Note that sediment layer thicknesses inside the pockmark are slightly thicker than outside the pockmark, as marked by double-headed arrows. See Figure 3 for location.

The craters of paleo-pockmarks showed noticeable basinward offset compared to present-day seafloor pockmarks in variance attribute maps (Figure 3, 10), indicating the craters of PM8 migrate from platform margin to slope direction. The sediment accumulated in the central region of PM8 is much thicker compared with that at marginal areas and the surrounding strata (Figure 14), which indicate syn-deformation or syn-slumping sediment processes during the genesis of pockmark (Anderson et al., 2008; Hovland et al., 2002).

For Peer Review

During the migration period during mature phase, the contour current may rework the architecture of pockmarks, especially for the crescent-like, elliptical, and irregular shape pockmarks (Su et al., 2011a; Anderson et al., 2008). The distribution of these pockmarks exhibits platform margin dominancy, where the bottom currents might be violent.

Abandonment stage

The abandonment, or burial, stage of pockmarks initiated after they ceased development, indicating the cessation of fluid migration caused by tectonic movements or sediment processes. Younger sediment, which is characterized by parallel seismic reflectors, filled pockmark depressions (Figure 15). Some pockmarks appear to have resumed activity, e.g., PM8, inheriting the previous structure (Figure

14). Others appear to have become dormant and been buried by thick younger sediments, so no longer appear as significant features on the seafloor (Figure 15).

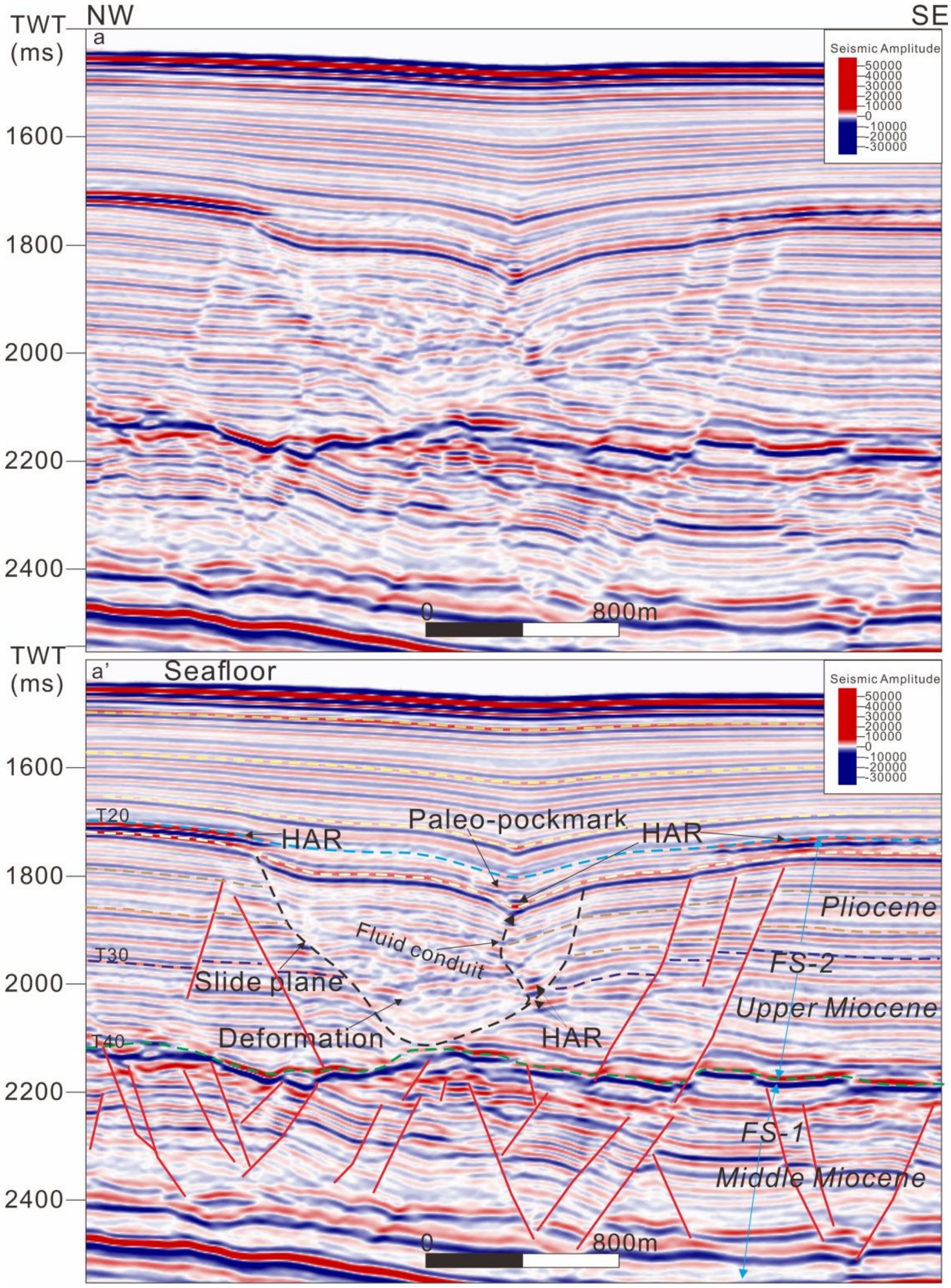

Figure 15 a) Seismic section across a buried paleo-pockmark. b) The same seismic section with interpretation. This pockmark developed in PFS-2, and has a typical funnel outline. There is no significant deformation in the shallow interval, and no significant depression on the seafloor. The inner filling sediment

was characterized by deformation of soft, fine-grained sediment, as captured by chaotic seismic reflectors. See Figure 3 for location.

Paleo-pockmarks exhibit no close relationship with present seafloor pockmarks. Funnel features of paleo-pockmark could easily be identified, which represent the main body of the paleo-pockmarks. The distinct boundaries between paleo-pockmarks and surrounding strata imply different depositional regimes. The lower part of pockmark exhibits lower frequency and amplitude reflection, with some fault-like features indicating sliding or slumping structure. The upper part of paleo-pockmark displays more gentle deformation than the lower part. The continuous HARs were interrupted at the top of the paleo-pockmarks, which are just close to the margin of pockmark. Meanwhile, the amplitude of HARs decreases far away pockmark. Another conduit and associated crater are identified in the main body of paleo-pockmark, with a series of HARs along the conduit as well as the top of pockmark. However, all the HARs terminate at T20, which represent the termination of Neogene. Above the T20, the intervals become horizontal, indicating cessation of fluid seepage. Therefore, the abandoned pockmark stopped developing at T20, then abandoned and buried by younger sediments.

Controlling factors on the mega-pockmark formation

Volcanisms

The close spatial relationship between volcanoes and volcano-associated pockmarks indicates that the volcanoes themselves provide a fluid source for the

For Peer Review

genesis of the pockmarks. The genesis of pockmarks related to diapirs are revealed and discussed in several other regions globally (Hovland and Judd, 1988; Hovland, 1991, 1992; Dimitrov and Woodside, 2003; Pilcher and Argent, 2007). The roots of the observed diapirs in previous study could reach down to the deep interval which provides fluid source. Therefore, the geo-fluids could migrate along diapirs, providing fluid source for formation of pockmarks in fine-grained soft sediment intervals above Middle Miocene (Hovland and Judd, 1988; Hovland, 1991, 1992; Dimitrov and Woodside, 2003; Pilcher and Argent, 2007).

However, the genesis and evolution of pockmarks related to volcanoes have not widely discussed yet. Previous study confirmed that the genesis and distribution of diatremes is controlled by the activities of volcanoes in offshore areas (Suiting and Schmincke, 2009, 2010, 2012; Go et al., 2017). The volcanic activities could deform the sediment intervals by both “hard intrusion” (Lu et al., 2011; Zhao et al., 2016; 2020) and “soft deformation”. The genesis of volcano-associated pockmarks in study area is closely related to “soft deformation”, which is dominated by fluid activities. The craters of most volcanoes are buried in subsurface, rather than reach to the seafloor. However, the fluid conduits, such as forced faults, could be identified in seismic section, which root on the crater of volcanoes. That implies the fluid from phreatomagmatic eruptions, such as gas and volcanic hydrothermal solutions, escaping from the volcanoes, seeping to seafloor. These fluids are essential for the genesis of pockmarks, as other pockmarks identified all around the world (Sun et al.,

For Peer Review

2011a; Cartwright, 2011; Chen et al., 2015). The sediment sequences inside volcano-associated pockmarks are comparable with the surrounding strata (Figure 14, 15), indicating the genesis of volcano-associated pockmarks lasts to very young age; that implies the volcanic activities could be very young.

Besides of central crater of volcano-associated pockmarks, secondary craters also develop on the seafloor (Figure 14). The secondary craters, exhibit ring-shape and distribute around the margin of volcano-associated pockmarks. The distribution of secondary craters implies that marginal sliding planes are also fluid conduits for the seepage of volcanic fluids. Meanwhile, the secondary craters imply the study area experiences multi-episode volcanic explosion events, which also create significant mega-pockmarks on the seafloor.

The fluids for the genesis of volcano-associated pockmarks escape from volcanoes, like a "point-source". The volcanoes releases gas and hydrothermal solutions from a constant point-like area, the fluid trends to escape in a limited area. Therefore, volcano-associated pockmarks are primarily circular and semi-circular shape, and exhibit great scale depression features on the seafloor (Figure 3, 5, 12).

Linear faults

The linear faults-associated pockmarks rooted on the top of Middle Miocene, where the NW-SE oriented linear faults densely develop. The Middle Miocene is significant carbonate reservoirs of petroleum system in study area (Lu et al., 2017; 2011). The coincidence between linear faults-associated pockmarks and linear faults

For Peer Review

underneath them indicates these linear faults acted as essential conduits for fluid escape (Pilcher and Argent, 2007). The development of NW-SE fault system controls the distribution of linear faults-associated pockmarks. The NW-SE fault system breaks the preservation condition of the fluid reservoirs in Middle Miocene, and provides migration path for the fluids. The fluid expulsion could occur when the balance between pore pressure and hydrostatic pressure is broken by tectonic or sedimentary events, such as sea level fall (Lafuerza et al., 2009; Plaza-Faverola et al., 2011; Nakajima et al., 2014). The frequent sea level changes during Neogene in adjacent area have been documented by the well studies, such as wells XK-1, XY-1 and CK-1 (Xie et al., 2006; Wu et al., 2016). The escaped fluid will seep to the seafloor through and along the linear faults, which caused the NW-SE direction elongating feature of linear faults-associated pockmarks (Figure 3, 10). The fluids for the genesis of pockmarks in study area mainly escape from linear faults, like a linear source. Comparing with the circular volcano-associated pockmarks, the differential fluid escaping pattern of linear faults-associated pockmarks creates diverse depression features on the seafloor.

The linear faults create central craters of the pockmarks, which subsequently lead to the slumps and slides in the margins of pockmarks (Figure 14, 16). The slumping and sliding events create slide planes which acted as secondary conduits at the margins of pockmarks, which form secondary craters inside the pockmarks (Figure 14, 16).

For Peer Review

The difference in sediment thickness between pockmarks and surrounding strata is subtle, allowing seismic reflectors with the pockmarks and the surrounding strata to be compared (Figure 12-15). Such comparison indicates that slumping and sliding comprise the major formation events (Hovland, 1982; Anderson, 2008). The fact that only minor differences are observed in the thickness of layers within pockmarks and the surrounding strata implies that the pockmarks accepts same sediment with the surrounding strata during their formation. The similar sediment between inside and outside of pockmarks also imply the linear faults are still active as the fluid seeps through them until present.

The slumping events inside pockmarks provide more space for sediment accumulation, as well as driving the sediment deformed. The several sediment sequences indicate the filling inside pockmarks experience several syn-slumping sediment periods.

Fluid source

The formation of pockmarks on the seafloor was generally controlled by two primary factors: the source of fluid, and the soft fine grained pelagic sediments that comprise the shallow intervals. The liquid fluid for genesis of pockmarks has been suggested to be water (Harrington, 1985), and the primary gas fluid suggested to be both biogenic gas and thermogenic gas (Davies et al, 1999; Owen, 2003; Rogers et al., 2006; Hartwig et al., 2012). Meanwhile, Gas hydrates have also been shown to play a significant role in the formation of pockmarks (Plaza-Faverola et al., 2011; Sun et al.,

For Peer Review

2012; Lu et al., 2017). The internal architecture of pockmarks and paleo-pockmarks indicate that all pockmarks have experienced long-term evolution. Long-term, multi-episode fluid expulsion events have resulted in complex morphologies, as well as the great scale of mega-pockmarks.

The fluid source for the genesis of volcano-associated and linear faults-associated pockmarks have different origins. For the linear faults-associated pockmarks, the linear faults act as fluid conduits for the migration of fluid source from deep intervals or surrounding intervals. In the study area, all pockmarks are located above top Middle Miocene, and most of them are associated with NW-SE linear faults (Figure 10, 16). This implies that the thermogenic gas and fluid sources at deeper intervals dominantly contribute to the formation of pockmarks.

Oligocene and Eocene source rocks are major source rocks for thermogenic gas in northwestern SCS, while Middle Miocene is significant carbonate reservoirs (Lu et al., 2011; 2017). The thermogenic gas could migrate from source kitchen into hydrocarbon reservoirs in shallower intervals through faults or other conduits (Lu et al., 2011; 2017). Besides thermogenic gas, the biogenic gas generated in shallow intervals also provide fluid source for genesis of pockmarks. The organic rich fine-grained muddy and silty sediments provided source rock for biogenic methane (Rice and Claypool, 1981; Hovland et al., 1993). The gas seeps in the northern slope of the SCS, Haima cold seeps adjacent study area, revealed a mixed gas source of biogenic and thermogenic gas, that could account for the formation of pockmarks

For Peer Review

(Huang et al. 2003; Chen et al., 2006; Zhu et al. 2009; Tong et al., 2013; Liang et al., 2017; Niu et al., 2017; Gong et al., 2018). Meanwhile, gas hydrates, formed either from thermogenic gas in deeper intervals or biogenic gas in shallow intervals, may also played a secondary role in the formation of pockmarks (Buffett, 2000; Boswell et al., 2012b; Boswell et al., 2016; Lu et al., 2017).

For the volcano-associated pockmarks, the fluid source for their development is more likely from the volcanic activities, such as gas and volcanic hydrothermal solutions, escaping from the phreatomagmatic eruptions (Figure 16).

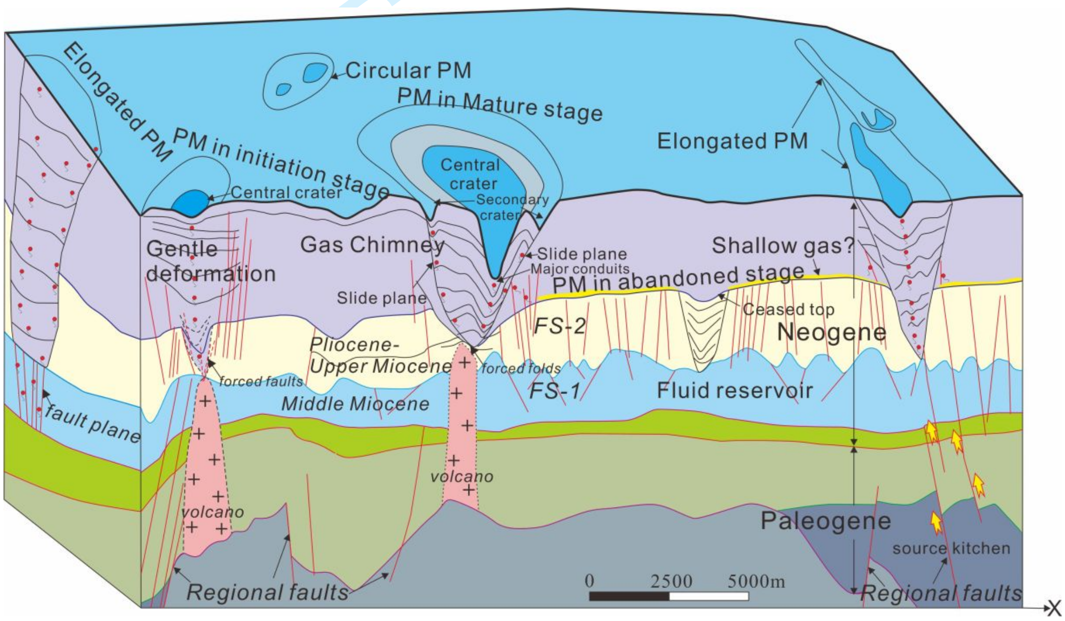

Figure 16 Schematic geological model showing the genesis of pockmarks of different styles. The different styles and shapes of pockmarks were derived from seismic sections. PPM: paleo-pockmark.

Conclusions

Mega-pockmarks and other fluid activity-related structures are identified and interpreted using high resolution 3D seismic images. The unique features of the mega-pockmarks are observed on the seafloor, and the internal architectures in the shallow subsurface are imaged by 3D seismic data. The initiation and evolution of mega-pockmarks recorded long-term and multi-episode fluid activity in the study area. The scale of mega-pockmarks indicates the complicated tectonic and sedimentary activities in northwest margin of SCS.

1. The pockmarks can be classified into two different categories, which are linear fault-associated pockmarks, and volcano-associated pockmarks. The polygonal fault-associated pockmarks exhibit elongating shape, and distribute abundantly in the east and west regions of the study area. The volcano-associated pockmarks are commonly circular shape, and develop in the southwest part of study area.

2. Initiation, mature and abandonment stages of pockmarks could be identified in seismic sections. The pockmarks in mature stage generally develop more than one crater. Long time and multi-episode fluid seepages lead to the great scale and complicated architecture of pockmarks.

3. The roots of linear faults-associated pockmarks generally reached the top of Middle Miocene, which is reservoir of petroleum system. The linear faults play significant roles in the migration of gas and fluids, and the genesis of pockmarks. The fluid sources for the genesis of volcano-associated pockmarks are mainly from the volcanic activities.

Acknowledgements

For Peer Review

We would like to thank Hangzhou Research Institute of Geology research team, especially the South China Sea team for their contributions, and the approval of this publication. This study was supported by the China ASEAN marine seismic data platform and Research Center (12120100500017001) and the National Natural Science Foundation of China (41676041 and 41276053).

References

Andresen, K. J., Huuse, M. 2011. “Bulls-eye” pockmarks and polygonal faulting in the Lower Congo Basin: Relative timing and implications for fluid expulsion during shallow burial. Mar. Geol. 279, 111–127. doi:10.1016/j.margeo.2010.10.016.

Andresen, K.J., Huusew, M., Clausenn, O. R., 2008. Morphology and distribution of Oligocene and Miocene pockmarks in the Danish North Sea - implications for bottomcurrent activity and fluid migration. Basin Research,20, 445-466.

Bertoni, C., Gan, Y. P., Paganoni, M., Mayer, J., Cartwright, J., Martin, J., Van Rensbergen, P., Wunderlich, A., Clare, A., 2019. Late Paleocene pipe swarm in the Great South–Canterbury Basin (New Zealand). Marine and Petroleum Geology, 107, 451-466.

Bøe, R., Rise, L., Ottesen, D., 1998. Elongate depressions on the southern slope of the Norwegian Trench (Skagerrak): morphology and evolution. Marine Geology 146, 191-203.

For Peer Review

Boswell, R., 2007, Resource potential of methane hydrate coming into focus. Journal of Petroleum Science and Engineering, 56, 9-13.

Boswell, R., Shipp, C., Reichel, T., Shelander, D., Saeki, T., Frye, M., Shedd, W., Collett, T. S., McConnell, D. R., 2016. Prospecting for marine gas hydrate resources. Interpretation 4, SA13-SA24.

Boswell, R., Frye, M., Shelander, D., Shedd, W., McConnelle, D. R., Cook, A., 2012a. Architecture of gas-hydrate-bearing sands from Walker Ridge 313, Green Canyon 955, and Alaminos Canyon 21: Northern deepwater Gulf of Mexico: Marine and Petroleum Geology 34, 134-149.

Boswell, R., Collett, T. S., Frye, M., Shedd, W., McConnell, D. R., Shelander, D., 2012b. Subsurface gas hydrates in the northern Gulf of Mexico. Marine and Petroleum Geology, 34, 4-30.

Buffett, B. A., 2000. Clathrate hydrates. Annual Review of Earth and Planetary Science 28, 477-507.

Cartwright, J., Santamarina, C., 2015. Seismic characteristics of fluid escape pipes in sedimentary basins: implications for pipe genesis. Marine and Petroleum Geology, 65, 126-140.

Cartwright, J. A., 2011. Diagenetically induced shear failure of fine-grained sediment sand the development of polygonal fault systems. Marine and Petroleum Geology, 28, 1593-1610.

Cartwright, J., Huuse, M., Aplin, A., 2007. Seal bypass systems. AAPG bulletin,

For Peer Review

91(8), 1141-1166.

Cartwright, J. A., James, D., Bolton, A., 2003. The genesis of polygonal fault systems: a review. In Van Rensbergen, P., Hillis, R. R., Maltman, A. J., Morley, C. K. (Eds), 2003. Subsurface Sediment Mobilization. Geological Society, London, Special Publications 216, 223-243.

Cartwright, J. A., 1999. Polygonal fault systems: a new type of fault structure revealed by 3-Dseismic data from the North Sea Basin. In Weimer P. and T. L. Davis, (Eds.), 1999. AAPG Studies in Geology No. 42 and SEG Geophysical Developments Series No. 5, AAPG/SEG, Tulsa, 225-230.

Cathles, L.M., Su, Z., Chen, D.F., 2010. The physics of gas chimney and pockmark formation, with implications for assessment of seafloor hazards and gas sequestration. Marine and Petroleum Geology 27, 82-91.

Chen, J. X., Song, H. B., Guan, Y. X., Yang, S. X., Pinheiro, L. M., Bai, Y., Liu, B. R., Geng, M. H., 2015. Morphologies, classification and genesis of pockmarks, mud volcanoes and associated fluid escape features in the northern Zhongjiannan Basin, South China Sea. Deep-Sea Research II 122, 106–117.

Chen, Z., Yan, W., Chen, M.H., Wang, S.H., Lu, J., Zhang, F., Xiang, R., Xiao, S.B., Yan, P., Gu, S.C., 2006. Discovery of seep carbonate nodules as new evidence for gas venting on the northern continental slope of South China Sea. Chinese Science Bulletin 51, 1228-1237.

Cole, D., Stewart, S.A., Cartwright, J.A., 2000. Giant irregular pockmark craters in

For Peer Review

the Palaeogene of the Outer Moray Firth Basin, UK North Sea. Mar. Pet. Geol. 17, 563–577.

Davies, R., Cartwright, J.A., Rana, J., 1999. Giant hummocks in deep-water marine sediments: evidence for large-scale differential compaction and density inversion during early burial. Geology 27, 907–910.

Decker, C., Olu, K., 2010. Does macrofaunal nutrition vary among habitats at the Håkon Mosby mud volcano? Cahiers De Biologie Marine, 51, 361–367.

Dimitrov, L.,Woodside, J., 2003. Deep sea pockmark environments in the eastern Mediterranean. Mar. Geol. 195, 263–276.

Fader, G.B.J., 1991. Gas-related sedimentary features from the eastern Canadian continental shelf. Cont. Shelf Res. 11, 1123–1153.

Foland, S.S., Maher, N., Yun, J.W., 1999. Pockmarks along the Californian Continental Margin: implications for fluid flow. Abstract. AAPG Bull. 83, 681–706.

Fyhn, M. B. W., Nielsen, L. H., Boldrell, L. O., Thang, L. D., Bojesen, K. J., Petersen, H. I., Huyen, N. T., Duc, N. A., Dau, N. T., Mathiesen, A., Reid, I., Huong, D. T., Tuan, H. A., Hien, L. V., Nytoft, H. P., batzis, I., 2009. Geological evolution, regional perspectives and hydrocarbon potential of the northwest Phu Khanh Basin, offshore Central Vietnam. Marine and Petroleum Geology 26, 1-24.

Gao, H.F., 2012. Seismic facies' characteristic of turbidites and sea level change in the northwest sub-basin of South China Sea since late Miocene (Chinese with English Abstract). Journal of Tropical Oceanography, 31(3), 113-119.

For Peer Review

Gay, A., Berndt, C., 2007. Cessation/reactivation of polygonal faulting and effects on fluid flow in the Vøring Basin, Norwegian margin. Journal of the Geological Society 164:129-141.

Gay, A, Lopez, M., Berndt, C., Séranne, M., 2007. Geological controls on focused fluid flow associated with seafloor seeps in the Lower Congo Basin. Marine Geology 244, 68–92.

Gay, A., Lopez, M., Cochonat, P., Sultan, N., Cauquil, E., Brigaud, F., 2003. Sinuous pockmark belt as indicator of a shallow buried turbiditic channel on the lower slope of the Congo basin, West African margin. In:Van Rensbergen, P., Hillis, R.R., Maltman, A.J., Morley, C.K. (Eds.), Subsurface Sediment Mobilization. Geol. Soc. Lond. Spec. Pub., vol. 216, pp. 173–189.

Gay, A., Lopez, M., Cochonat, P., Levache, D., Sermondadaz, G., Séranne, M., 2006a. Evidences of early to late fluid migration from an upper Miocene turbiditic channel revealed by 3D seismic coupled to geochemical sampling within seafloor pockmarks, Lower Congo Basin. Marine and Petroleum Geology 23, 387-399.

Gay, A., Lopez, M., Cochonat, P., Séranne, M., Levaché, D., Sermondadaz, G., 2006b. Isolated seafloor pockmarks linked to BSRs, fluid chimneys, polygonal faults and stacked Oligocene–Miocene turbiditic palaeo channels in the Lower Congo Basin. Marine Geology 226, 25–40.

Gong, S.G., Hu, Y., Li, N., Feng, D., Liang, Q.Y., Tong H.P., Peng, Y.B., Tao, J., Chen, D.F., 2018. Environmental controls on sulfur isotopic compositions of

For Peer Review

sulfide minerals in seep carbonates from the South China Sea. Journal of Asian Earth Sciences, https://doi.org/10.1016/j.jseaes.2018.04.037.

Gong, Z.S., 1997, The Major Offshore Oil and Gas Fields in China: Petroleum Industry Press, Beijing (in Chinese with English abstract).

Hammer, O., Webb, K. E., 2010. Piston coring of Inner Oslo fjord Pockmarks, Norway: constraints on age and mechanism. Nor. J. Geol. 90, 79–91.

Haq, B.U., Hardenbol, J., VAIL, P. R., 1987. Chronology of fluctuating sea levels since the Triassic. Science 235, 1156–1167.

Harrington, P.K., 1985. Formation of pockmarks by pore-water escape. Geo-Marine Letters 5, 193-197.

Harris, P.T.; Baker, E.K., 2012. Seafloor Geomorphology as Benthic Habitat, 1st ed.; Elsevier: London, UK; p. 900.

Hartwig A, Anka Z, di Primio R, 2012. Evidence of a widespread paleo-pockmarked field in the Orange Basin: an indication of an early Eocene massive fluid escape event offshore South Africa. Marine Geology, 332: 222-234.

Haskell, N., Grindhaug, J., Dhanani, S., Heath, R., Kantorowicz, J., Antrim, L., Cubanski,M., Nataraj, R., Schilly,M.,Wigger, S., 1999. Delineation of geological drilling hazards using 3-D seismic attributes. Leading Edge, 18, 373–382.

Hovland, M., 1982. Pockmarks and the recent geology of the central section of the Norwegian Trench. Marine Geology, 47, 283-301.

For Peer Review

Hovland, M., Judd, A.G., 1988. Seabed Pockmarks and Seepages. Impact on Geology, Biology and the Marine Environment. Graham & Trotman, London. 293 pp.

Hovland, M., 1991. Large Pockmarks, gas-charged sediments and possible clay diapirs in the Skagerrak. Marine and Petroleum Geology, 8, 311–316.

Hovland, M., 1992. Hydrocarbon seeps in northern marine waters -their occurrence and effects. Palaeios 7, 376–382.

Hovland, M., Judd, A. G., Burke Jr. R. A., 1993. The global flux of methane from shallow submarine sediments. Chemosphere 26, 559–578.

Hovland, M., Gardner, J. V., Judd, A.G., 2002. The significance of pockmarks to understanding fluid flow processes and geohazards. Geofluids 2, 127-136. doi:10.1046/j.1468-8123.2002.00028.x

Huang, B. J., Xiao, X. M., Zhang, M. Q., 2003. Geochemistry, grouping and origins of crude oils in the Western Pearl River Mouth Basin, offshore South China Sea: Organic Geochemistry 34, 993-1008.

Judd, A. G., Hovland, M., Dimitrov, L. I., Garca Gil, S., Jukes, V., 2002. The geological methane budget at continental margins and its influence on climate change. Geofluids2, 109–126.

Judd, A.G., Hovland, M., 2009. Seabed Fluid Flow: The Impact on Geology, Biology and the Marine Environment; Cambridge University Press: Cambridge, UK, 2007; p. 475.

King, L.H., MacLean, B., 1970. Pockmarks on the Scotian shelf. Geological Society

For Peer Review

of America Bulletin, 81, 3141–3148.

Krämer, K., Holler, P., Herbst, G., Bratek, A., Ahmerkamp, S., Neumann, A., Winter, C., 2017. Abrupt emergence of a large pockmark field in the German Bight, southeastern North Sea. Scientific reports, 7(1), 5150.

Lafuerza, S., N. Sultan, M. Canals, J. Frigola, S. Berné, G. Jouet, M. Galavazi, and F. J. Sierro, 2009. Overpressure within upper continental slope sediments from CPTU data, Gulf of Lion, NW Mediterranean Sea. International Journal of Earth Sciences, 98(4), 751–768. doi:10.1007/s00531-008-0376-2.

Liang, Q.Y., Hu, Y., Feng, D., Peckmann, J., Chen, L.Y., Yang, S.X., Liang, J.Q., Tao, J., Chen, D.F., 2017. Authigenic carbonates from newly discovered active cold seeps on the northwestern slope of the South China Sea: Constraints on fluid sources, formation environments, and seepage dynamics. Deep-Sea Research Part I, 124, 31–41.

Lu, Y.T., Wang, B., Lü, F. L., He, X. S., Fan, G. Z., Wu, J. W., 2011. Basin Evolution and Petroleum Prospecting Potential of Deepwater Sedimentary Basins around Xisha Islands (In Chinese with English abstract). Marine Origin Petroleum Geology, 16, 32-38.

Lu, Y.T., Luan, X.W., Lyu, F.L., Wang, B., Yang, Z.L., Yang, T.T., Yao, G.S., 2017. Seismic evidence and formation mechanism of gas hydrates in the Zhongjiannan Basin, Western margin of the South China Sea. Marine and Petroleum Geology, 84, 274-288.

For Peer Review

Lüdmann, T. Wong, H. K., 1999. Neotectonic regime at the passive continental margin of the northern South China Sea. Tectonophysics 311, 113-138.

Lüdmann, T., Wong, H. K., Kai, B., 2005. Upward flow of North Pacific Deep Water in the northern South China Sea as deduced from the occurrence of drift sediments: Geophysical Research Letters, 32, 215-236.

Ma, Y. B., Wu, S. G., Lv, F. L., Dong, D. D., Sun, Q. L., Lu, Y. T., Gu, M. F., 2011. Seismic characteristics and development of the Xisha carbonate platforms, northern margin of the South China Sea. Journal of Asian Earth Sciences 40, 770–783.

Maestrelli, D., Iacopini, D., Jihad, A. A., Bond, C. E., Bonini, M., 2017. Seismic and structural characterization of fluid escape pipes using 3D and partial stack seismic from the Loyal Field (Scotland, UK): A multiphase and repeated intrusive mechanism. Marine and Petroleum Geology, 88, 489-510.

Mazzini, A., Svensen, H.H., Forsberg, C.F., Linge, H., Lauritzen, S.E., Haflidason, H., Hammer, Ø., Planke, S., Tjelta, T.I., 2017. A climatic trigger for the giant Troll pockmark field in the northern North Sea. Earth Planet Science Letter 464, 24-34. doi:10.1016/j.epsl.2017.02.014.

Miller, K.G., Kominz, M.A., Browning, J.V., Wright, J.D., Mountain, G.S., Katz, M.E., Sugarman, P.J., Cramer, B.S., Christie-Blick, N., Pekar, S.F., 2005. The Phanerozoic record of global sea-level change. Science 310, 1293-1299.

Moss, J. L., & Cartwright, J. (2010). 3D seismic expression of km-scale fluid escape

For Peer Review

pipes from offshore Namibia. Basin Research, 22(4), 481-501.

Nakajima, T., Kakuwa, Y., Yasudomi, Y., Itaki, T., Motoyama, I., Tomiyama, T., Machiyama, H., Katayama, H., Okitsu, O., Morita, S., Tanahashi, M., Matsumoto, R., 2014. Formation of pockmarks and submarine canyons associated with dissociation of gas hydrates on the Joetsu Knoll, eastern margin of the Sea of Japan. Journal of Asian Earth Sciences 90, 228-242.

Nicholas, W.A., Carroll, A., Picard, K., Radke, L., Siwabessy, J., Chen, J., Howard, F.J.F., Dulfer, H.,Tran, M., Consoli, C., Przeslawski, R., Li, J., Jones, L.E.A. 2015. Seabed environments, shallow sub-surface geology and connectivity, Petrel Sub-basin, Bonaparte Basin, Timor Sea: Interpretative report from marine survey GA0335/SOL5463. Record 2015/24. Geoscience Australia, Canberra: p. 124. http://dx.doi.org/10.11636/Record.2015.024.

Niu, M.Y., Fan, X.B., Zhuang G.C., Liang Q.Y., Wang F.P., 2017. Methane-metabolizing microbial communities in sediments of the Haima cold seep area, northwest slope of the South China Sea. FEMS Microbiology Ecology, 93, 1-13.

Owen, G., 2003. Load structures: gravity-driven sediment mobilization in the shallow subsurface. Geological Society, London, Special Publications 216, 21–34.

Picard, K., Radke, L., Williams, D., Nicholas, W., Siwabessy, P., Howard, F., Gafeira, J., Przeslawski, R., Huang, Z., Nichol, S., 2018. Origin of High Density Seabed

For Peer Review

Pockmark Fields and Their Use in Inferring Bottom Currents. Geosciences 195, 1-23. doi:10.3390/geosciences8060195.

Pilcher, R., Argent, J., 2007. Mega-pockmarks and linear pockmark trains on the West African continental margin. Marine Geology 244, 15-23.

Plaza-Faverola, A., Bünz, S., Mienert, J., 2011. Repeated fluid expulsion through sub-seabed chimneys offshore Norway in response to glacial cycles. Earth Planetary. Science Letters, 305, 297–308. doi:10.1016/j.epsl.2011.03.001.

Riboulot, V., Cattaneo, A., Sultan, N., Garziglia, S., Ker, S., Imbert, P., Voisset, M., 2013. Sea-level change and free gas occurrence influencing a submarine landslide and pockmark formation and distribution in deepwater Nigeria. Earth Planet. Sci. Lett. 375, 78–91.

Riboulot, V., Thomas, Y., Berné, S., Jouet, G., Cattaneo, A., 2014. Control of Quaternary sea-level changes on gas seeps. Geophys. Res. Lett. 41, 4970–4977. doi:10.1002/2014GL060460.

Rice, D. D., Claypool, G. E., 1981. Generation, accumulation and resource potential of biogenic gas. AAPG Bull. 65, 5–25.

Rollet, N., Logan, G. A., Kennard, J. M., O’Brien, P. E., Jones, A. T., Sexton, M., 2006. Characterisation and correlation of active hydrocarbon seepage using geophysical data sets: an example from the tropical, carbonate Yampi Shelf, Northwest Australia. Mar. Pet. Geol. 23, 145–164.

Rowan, M.G., Jackson, M.P.A., Trudgill, B.D., 1999. Salt-related fault families and

For Peer Review

fault welds in the northern Gulf of Mexico. AAPG Bull. 83, 1454-1484.

Sun, Q. L., Wu, S. G., Yao, G. S., Lü, F. L., 2009. Characteristics and Formation Mechanism of Polygonal Faults in Qiongdongnan Basin, Northern South China Sea. Journal of Earth Science 20, 180–192.

Sun, Q. L., Wu, S. G., Lü, F.L., Yuan, S. Q., 2010. Polygonal faults and their implications for hydrocarbon reservoirs in the southern Qiongdongnan Basin, South China Sea. Journal of Asian Earth Science 39, 470-479.

Sun, Q. L., Wu, S. G., Hovland, M., Luo, P., Lu, Y. T., Qu, T., 2011a. The morphologies and genesis of mega-pockmarks near the Xisha Uplift, South China Sea. Marine and Petroleum Geology 28, 1146-1156.

Sun, Q. L., Wu, S. G., Lüdmann, T., Wang, B., Yang, T. T., 2011b. Geophysical evidence for cyclic sediment deposition on the southern slope of Qiongdongnan Basin, South China Sea. Marine Geophysical Researches 32, 415-428.

Sun, Q. L., Wu, S. G., Cartwright, J., Dong, D. D., 2012a. Shallow gas and focused fluid flow systems in the Pearl River Mouth Basin, northern South China Sea. Marine Geology 315-318, 1-14.

Sun, Y. B., Wu, S. G., Dong, D. D., Lüdmann, T., Gong, Y. H., 2012b. Gas hydrates associated with gas chimneys in fine-grained sediments of the northern South China Sea. Marine Geology 311-314, 32–40.

Sun, Q. L., Wu, S. G., Joseph, C., Lüdmann, T., Yao, G. S., 2013. Focused fluid flow systems of the Zhongjiannan Basin and Guangle Uplift, South China Sea. Basin

For Peer Review

Research 25, 97-111.

Tasianas, A., Bünz, S., Bellwald, B., Hammer, Ø., Planke, S., Lebedeva-Ivanova, N., Krassakis, P., 2018. High-resolution 3D seismic study of pockmarks and shallow fluid flow systems at the Snøhvit hydrocarbon field in the SW Barents Sea. Marine Geology, 403, 247-261.

Tjelta, T.I., Svanø, G., Strout, J.M., Forsberg, C.F., Planke, S., Johansen, H., 2007. Gas seepage and pressure build-up at a North Sea platform location: Gas origin, transportation, and potential hazards. In Proceedings of the Offshore Technology Conference (OTC), Houston, TX, USA, 30 April–4 May 2007; p. 11, OTC paper no.18699.

Tong, H.P., Feng, D., Cheng, H., Yang, S.X., Wang, H.B., Min, A.G., Edwards, R.L., Chen, Z., Chen, D.F., 2013. Authigenic carbonates from seeps on the northern continental slope of the South China Sea: New insights into fluid sources and geochronology. Marine and Petroleum Geology 43, 260-271.

Wrona T, Magee C, Jackson CA-L, Huuse M and Taylor KG (2017). Kinematics of Polygonal Fault Systems: Observations from the Northern North Sea. Frontiers in Earth Science, 5: 101.

Wang, X. J., Wu, S. G., Yuan, S. Q., Wang, D. W., Yao, G. S., Gong, Y., Zhang, G. X., 2010. Geophysical signatures associated with fluid flow and gas hydrate occurrence in a tectonically quiescent sequence, Qiongdongnan Basin, South China Sea. Geofluids10, 351-368.

For Peer Review

Wenau, S., Spieß, V., Pape, T., Fekete, N., 2017. Controlling mechanisms of giant deep water pockmarks in the Lower Congo Basin. Marine and Petroleum Geology, 83, 140-157. doi:10.1016/j.marpetgeo.2017.02.030.

Whelan, J., Eglinton, L., Cathles Iii, L., Losh, S., Roberts, H., 2005. Surface and subsurface manifestations of gas movement through a NeS transect of the Gulf of Mexico. Marine and Petroleum Geology, 22, 479-497.

Wu, F., Guo, L.Y., Zhnag, D.J., Xie, X.N., You, L., Du, X.B., 2016. High resolution sequence units division based on geochemical data: Taking Quaternary reef-bank strata of well XK1 as an example (Chinese with English abstract). Geological Science and Technology Information, 35(5), 42-51.

Xie, X. N., Müller, R. D., Li, S. T., Gong, Z. S., Steinberger, B., 2006. Origin of the anomalous subsidence along the Northern South China Sea margin and its relationship to dynamic topography. Marine and Petroleum Geology 23, 745-765.

Yan, P., Deng, H., Liu, H. L., Zhang, Z. R., Jiang, Y. K.. 2006. The temporal and spatial distribution of volcanism in the South China Sea region. Journal of Asian Earth Science 27, 647-659.

Zhao, Fang, Alves, Tiago M, Wu, Shiguo, Li, Wei, Huuse, Mads, Mi, Lijun, Sun, Qiliang and Ma, Benjun 2016. Prolonged post-rift magmatism on highly extended crust of divergent continental margins (Baiyun Sag, South China Sea). Earth and Planetary Science Letters 445 , pp. 79-91.

For Peer Review

doi:10.1016/j.epsl.2016.04.001.

Zhao, Fang, Alves, Tiago M., Xia, Shaohong, Li, Wei, Wang, Lei, Mi, Lijun, Wu, Shiguo, Cao, Jinghe and Fan, Chaoyan 2020. Along-strike segmentation of the South China Sea margin imposed by inherited pre-rift basement structures. Earth and Planetary Science Letters 530, 115862. doi: 10.1016/j.epsl.2019.115862.

Zhao, Q.H., Jian, Z.M., Wang, J.L., Cheng, X.R., Huang, B.Q., Xu, J., Zhou, Z., Fang, D.Y., Wang, P.X., 2001. Neogene oxygen isotopic stratigraphy, ODP Site 1148, northern South China Sea. Science in China (Series D) 44, 934-542.

Zhou, D., Ru, K., Chen, H. Z., 1995. Kinematics of Cenozoic extension on the South China Sea continental margin and its implications for the tectonic evolution of the region. Tectonophysics 251, 161-177.

Zhu, W. L., Huang, B. J., Mi, L. J., Wilins, R. W. T., Fu, N., Xiao, X. M., 2009. Geochemistry, origin, and deep-water exploration potential of natural gases in the Pearl River Mouth and Qiongdongnan basins, South China Sea. American Association of Petroleum Geologists Bulletin 93, 741-761.

For Peer Review